The DNA–Esperamicin A_1 Complex. A Model Based on Solvated Molecular Dynamics Simulations

D. R. Langley,*,†,‡ J. Golik,† B. Krishnan,† T. W. Doyle,† and D. L. Beveridge‡

Contribution from the Pharmaceutical Research Institute, Bristol-Myers Squibb Company, 5 Research Parkway, P.O. Box 5100, Wallingford, Connecticut 06492-7660, and Hall-Atwater Laboratories, Chemistry Department, Wesleyan University, Middletown, Connecticut 06457

*Received December 8, 1992. Revised Manuscript Received June 25, 1993**

Abstract: A solvated model for the DNA–esperamicin complex has been constructed and shown to be thermodynamically stable over a 300-ps molecular dynamics simulation. The dynamical model is consistent with all of the available experimental data. The model has been used to gain insights into (1) how esperamicin is activated into a DNA-cleaving molecule, (2) its mode of binding to DNA, (3) how the individual esperamicin residues contribute to its ability to bind with and cleave DNA, (4) the fate of the carbon-centered radicals, and (5) its DNA-cleavage patterns and cleavage sequence specificity. Furthermore, a comparison of the models for the DNA–esperamicin A_1 and DNA–esperamicin C complexes has been carried out to gain an understanding at the molecular level of the difference in the DNA-cutting abilities exhibited by these two esperamicin analogs. Finally, experimental data are presented that show that esperamicin A_1 undergoes fragmentation in the DNA-cleavage reaction. The DNA–esperamicin model has been used to provide a mechanistic rationale for the fragmentation reaction.

Introduction

Esperamicin A_1 (BMY-28175, Figure 1) is a metabolite of *Actinomadura verrucosospora*,[1] which was isolated from a soil sample collected at Pto Esperanza, Misions, Argentina. The esperamicins are members of the enediyne class of natural products, which includes neocarzinostatin,[2-9] the calicheamicins[10-13] (Figure 2), the dynemicins,[14-17] and kedarcidin.[18-24]

The initial fermentation yields of <1 μg/mL for esperamicin A_1 have seen a 50-fold improvement.[25] This has made it possible to produce adequate quantities of material for structure elucidation, mechanism of action, and advanced biological studies.

Esperamicin A_1 and related esperamicins (Figure 1) have been isolated, and their structures have been characterized.[26-28] Through a series of spectroscopic, X-ray, and synthetic studies, the structure and absolute stereochemistry for esperamicin A_1 have been determined.[29-34] It consists of a bicyclo[7.3.1] ring system (CORE, Figure 1) to which is attached a trisaccharide and a 2-deoxy-L-fucose (DF)–anthranilate (AC) moiety. The trisaccharide contains an unusual hydroxyamino sugar (HAS) which is attached to the CORE C8 via a glycosidic linkage. The hydroxyamino sugar is further linked to an isopropylamino sugar

† Bristol-Myers Squibb Co.
‡ Wesleyan University.
* Abstract published in *Advance ACS Abstracts*, November 15, 1993.

(1) Konishi, M.; Ohkuma, H.; Saitoh, K.-I.; Kawaguchi, H. *J. Antibiot.* **1985**, *38*, 1605–1609.
(2) Goldberg, I. H. *Acc. Chem. Res.* **1991**, *24*, 191–198.
(3) Edo, K.; Mizugaki, M.; Koide, Y.; Seto, H.; Furihata, K.; Otake, N.; Ishida, N. *Tetrahedron Lett.* **1985**, *26*, 331.
(4) Hensons, O. D.; Goldberg, I. H. *J. Antibiot.* **1989**, *42*, 761–768.
(5) Hensons, O. D.; Giner, J. L.; Goldberg, I. H. *J. Am. Chem. Soc.* **1989**, *111*, 3295–3299.
(6) Myers, A. G.; Proteau, P. J.; Handel, T. M. *J. Am. Chem. Soc.* **1988**, *110*, 7212.
(7) Dedon, P. C.; Goldberg, I. H. *Biochemistry* **1992**, *31*, 1909–1917.
(8) Dedon, P. C.; Jiang, Z.-W.; Goldberg, I. H. *Biochemistry* **1992**, *31*, 1917–1927.
(9) Adjadj, E.; Quiniou, E.; Mispelter, J.; Favaudon, V.; Lhoste, J.-M. *Eur. J. Biochem.* **1992**, *203*, 505–511.
(10) Lee, M. D.; Dunne, T. S.; Siegal, M. M.; Chang, C. C.; Morton, G. O.; Borders, D. B. *J. Am. Chem. Soc.* **1987**, *109*, 3464–3466.
(11) Lee, M. D.; Dunne, T. S.; Chang, C. C.; Ellestad, G. A.; Siegel, M. M.; Morton, G. O.; McGahren, W. J.; Borders, D. B. *J. Am. Chem. Soc.* **1987**, *109*, 3466–3468.
(12) Lee, M. D.; Manning, J. K.; Williams, D. R.; Kunk, N. A.; Testa, R. T.; Borders, D. B. *J. Antibiot.* **1989**, *42*, 1070–1087.
(13) Lee, M. D.; Dunne, T. S.; Chang, C. C.; Siegel, M. M.; Morton, G. O.; Ellestad, G. A.; McGahren, W. J.; Borders, D. B. *J. Am. Chem. Soc.* **1992**, *114*, 985–997.
(14) Konishi, M.; Ohkuma, H.; Matsumoto, K.; Tsuno, T.; Kamei, H.; Miyaki, T.; Oki, T.; Kawaguchi, H.; VanDuyne G. D.; Clardy, J. *J. Antibiot.* **1989**, *42*, 1449–1452.
(15) Konishi, M.; Ohkuma, H.; Tsuno, T.; Oki, T.; VanDuyne, G. D.; Clardy, J. *J. Am. Chem. Soc.* **1990**, *112*, 3715–3716.
(16) Langley, D. R.; Doyle, T. W.; Beveridge, D. L. *J. Am. Chem. Soc.* **1991**, *113*, 4395–4403.
(17) Tokiwa, Y.; Miyoshi-Saitoh, M.; Kobayashi, H.; Sunaga, R.; Konishi, M.; Oki, T.; Iwasaki, S. *J. Am. Chem. Soc.* **1992**, *114*, 4107–4110.
(18) Lam, K. S.; Hesler, G. A.; Gustavson, D. R.; Crosswell, A. R.; Veitch, J. M.; Forenza, S.; Tomita, K. *J. Antibiot.* **1991**, *44*, 472–478.
(19) Hofstead, S. J.; Matson, J. A.; Malacko, A. R.; Marquardt, H. *J. Antibiot.* **1992**, *45*, 1250–1254.
(20) Hofstead, S. J.; Matson, J. A.; Lam, K. S.; Forenza, S.; Bush, J. A.; Tomita, K. U.S. Patent 5,001,112, March 19, 1991.
(21) Leet, J. E.; Schroeder, D. R.; Hofstead, S. J.; Golik, J.; Colson, K. L.; Huang, S.; Klohr, S. E.; Doyle, T. W.; Matson, J. A. *J. Am. Chem. Soc.* **1992**, *114*, 7946–7948.
(22) Leet, J. E. U.S. Patent 5,143,906, Sept 1, 1992.
(23) Leet, J. E.; Golik, J.; Hofstead, S. J.; Matson, J. A.; Lee, A. Y.; Clardy, J. *Tetrahedron Lett.* **1992**, *33*, 6107–6110.
(24) Leet, J. E.; Schroeder, D. R.; Langley, D. R.; Hofstead, S. J.; Golik, J.; Colson, K. L.; Huang, S.; Klohr, S. E.; Lee, M. S.; Doyle, T. W.; Matson, J. A. *J. Am. Chem. Soc.* **1993**, *115*, 8432.
(25) Lam, K. S.; Forenza, S.; Veitch, J. A.; Gustavson, D. R.; Golik, J.; Doyle, T. W. Progress in Esperamicin Research. In *Novel Microbial Products for Medicine and Agriculture*; Nash, C. H., Demain, A. L., Hunter-Cevera, J. C., Eds.; William C. Brown Publishers: Dubuque, IA, 1992; Vol. 2, in press.
(26) Golik, J.; Clardy, J.; Dubay, G.; Groenewold, G.; Kawaguchi, H.; Konishi, M.; Krishnan, B.; Ohkuma, H.; Saitoh, K. I.; Doyle, T. W. *J. Am. Chem. Soc.* **1987**, *109*, 3461–3462.
(27) Golik, J.; Dubay, G.; Groenewold, G.; Kawaguchi, H.; Konishi, M.; Krishnan, B.; Ohkuma, H.; Saitoh, K. I.; Doyle, T. W. *J. Am. Chem. Soc.* **1987**, *109*, 3462–3464.
(28) Golik, J.; Beutler, J. A.; Clark, P.; Ross, J.; Roach, J.; Lebherz, W. B., III; Muschik, G. Applied U.S. Patent USSN323648, 1989.
(29) Golik, J.; Wong, H.; Vyas, D. M.; Doyle, T. W. *Tetrahedron Lett.* **1989**, *30*, 2497–2500.
(30) Whitman, M. D.; Halcomb, R. L.; Danishefsky, S. J.; Golik, J.; Vays, D. M. *J. Org. Chem.* **1990**, *55*, 1979–1981.
(31) Golik, J.; Doyle, T. W.; VanDuyne, G.; Clardy, J. *Tetrahedron Lett.* **1990**, *43*, 6149–6150.
(32) Halcomb, R. L.; Whitman, M. D.; Olson, S. H.; Danishefsky, S. J.; Golik, J.; Wong, H.; Vyas, D. M. *J. Am. Chem. Soc.* **1991**, *113*, 5080–5082.
(33) Golik, J.; Wong, H.; Krishnan, B.; Vyas, D. M.; Doyle, T. W. *Tetrahedron Lett.* **1991**, *32*, 1851–1854.
(34) Golik, J.; Krishnan, B.; Doyle, T. W. VanDuyne, G.; Clardy, J. *Tetrahedron Lett.* **1992**, *41*, 6049–6052.

0002-7863/94/1516-0015$04.50/0

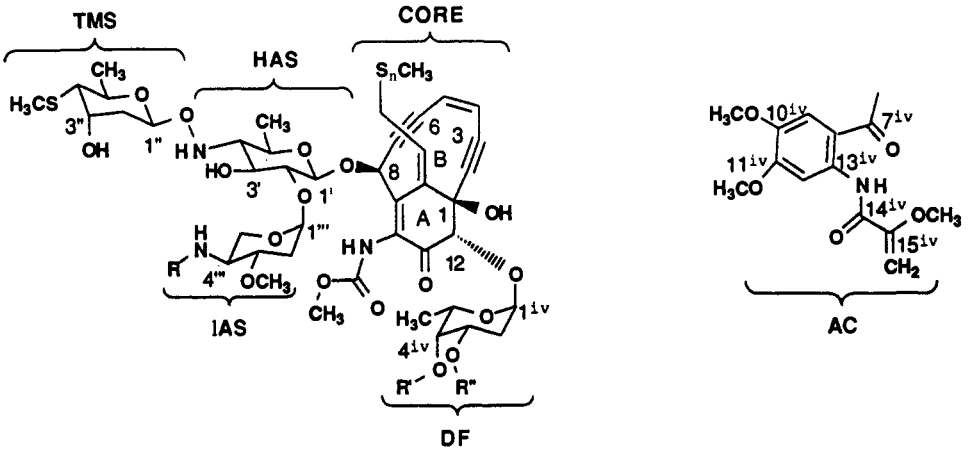

Esperamicin	n	R	R'	R''
A_1	3	$CH(CH_3)_2$	H	AC
A_{1b}	3	CH_2CH_3	H	AC
A_{1c}	3	CH_3	H	AC
P	4	$CH(CH_3)_2$	H	AC
A_2	3	$CH(CH_3)_2$	AC	H
A_{2b}	3	CH_2CH_3	AC	H
A_{2c}	3	CH_3	AC	H

Figure 1. Naturally occurring esperamicins.

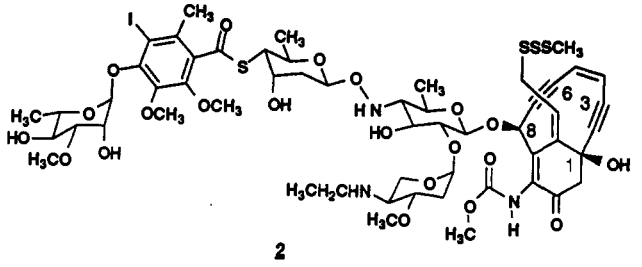

2

Figure 2. Calicheamicin γ_1^1.

(IAS) at C2′ through a glycosidic linkage and to a thiomethyl sugar (TMS) at C4′ by an unusual NO–glycosidic linkage. The CORE contains a 1,5-diyn-3-ene (diradical generator[27,35,36]), an allylic trisulfide, and a bridgehead enone.

Esperamicin A_1 is one of the most potent antitumor antibiotics known to man and has inhibitory activity against a wide range of murine and human tumor cell lines in both ip–ip and distal tumor models.[37,38] IC_{50} values in the ng/mL range are common. The HCT116 human colon carcinoma cell line is one of the most sensitive to esperamicin A_1 with an IC_{50} value of 300 pg/mL. Using alkaline elution techniques, breaks were detected in the DNA of HCT116 cells after a 1-h exposure with esperamicin A_1 at concentrations as low as 1 pg/mL. *In vitro* studies showed that esperamicin's ability to induce DNA strand breaks is dramatically enhanced in the presence of mild reducing agents,[37,39] and unlike the calicheamicins,[40–49] it produces predominantly single strand breaks.[37,39,50–57] As esperamicin A_1 is stepwise degraded from the parent compound through esperamicins C and D to E, its ability to bind with and cleave DNA is gradually reduced by approximately 5–6 orders of magnitude,[37] thus demonstrating the importance of each of the esperamicin residues in producing a highly efficient DNA-cleaving agent. On the basis of esperamicin's unusual structure, extreme potency, wide spectrum of activity, novel mechanism of action, and distal tumor activity, it was selected as a clinical candidate.

Esperamicin A_1 has successfully completed phase I (safety) trials.[58] Phase II (efficacy) trials are now under way in the U.S. and Europe.

The mechanism by which esperamicin produces its biological effects has been attributed to its ability to complex with and

(35) Lockart, T. P.; Comita, P. B.; Bergman, R. G. *J. Am. Chem. Soc.* **1981**, *103*, 4082–4090.
(36) Bergman, R. G. *Acc. Chem. Res.* **1973**, *6*, 25–31.
(37) Long, B. H.; Golik, J.; Forenza, S.; Ward, B.; Rehfuss, R.; Dabrowiak, J. C.; Catino, J. J.; Musial, S. T.; Brookshire, K. W.; Doyle, T. W. *Proc. Natl. Acad. Sci. U.S.A.* **1989**, *86*, 2–6.
(38) Schurig, J. E.; Rose, W. C.; Kamei, H.; Nishiyama, Y.; Bradner, W. T.; Stringfellow, D. A. *Invest. New Drugs* **1990**, *8*, 7–15.
(39) Suglura, Y.; Uesawa, Y.; Takahashi, Y.; Kuwahara, J.; Golik, J.; Doyle, T. W. *Proc. Natl. Acad. Sci. U.S.A.* **1989**, *86*, 7672–7676.
(40) Zein, N.; Sinha, A. M.; McGahren, W. J.; Ellestad, G. A. *Science* **1988**, *240*, 1198–1201.
(41) Zein, N.; Poncin, M.; Nilakatan, R.; Ellestad, G. A. *Science* **1989**, *244*, 697–669.
(42) De Voss, J. J.; Townsend, C. A.; Ding, D.-W.; Morton, G. O.; Ellestad, G. A.; Zein, N.; Tabor, A. B.; Schreiber, S. L. *J. Am. Chem. Soc.* **1990**, *112*, 9670–9671.
(43) Drak, J.; Iwasawa, N.; Danishefsky, D.; Crothers, D. M. *Proc. Natl. Acad. Sci. U.S.A.* **1991**, *88*, 7464–7468.
(44) Walker, S.; Landovitz, R.; Ding, W.-D.; Ellestad, G. A.; Kahne, D. *Proc. Natl. Acad. Sci. U.S.A.* **1992**, *89*, 4608–4612.
(45) Aiyar, J.; Danishefsky, S. J.; Crothers, D. M. *J. Am. Chem. Soc.* **1992**, *114*, 7552–7554.
(46) Nicolaou, K. C.; Tsay, S.-C.; Suzuki, T.; Joyce, G. F. *J. Am. Chem. Soc.* **1992**, *114*, 7555–7557.
(47) Zein, N.; McGahren, W. J.; Morton, G. O.; Ashcroft, J.; Ellestad, G. A. *J. Am. Soc.* **1989**, *111*, 6888–6890.
(48) Hangeland, J. J.; De Voss, J. J.; Heath, J. A.; Townsend, C. A.; Ding, W.; Ashcroft, J. S.; Ellestad, G. A. *J. Am. Chem. Soc.* **1992**, *114*, 9200–9202.
(49) Nicolaou, K. C.; Dai, W.-M. *Angew. Chem., Int. Ed. Engl.* **1991**, *30*, 1387–1416.
(50) Kozarich, J. W.; Worth, L., Jr.; Frank, B. L.; Christner, D. F.; Vanderwall, D. E.; Stubbe, J. *Science* **1989**, *245*, 1396–1399.
(51) Uesawa, Y.; Kuwahara, J.; Sugiura, Y. *Biochem. Biophys. Res. Commun.* **1989**, *164*, 903–911.
(52) Kishikawa, H.; Jiang, Y.-P.; Goodisman, J.; Dabrowiak, J. C. *J. Am. Chem. Soc.* **1991**, *113*, 5434–5440.
(53) Kishikawa, H.; Jiang, Y.-P.; Goodisman, J.; Dabrowiak, J. C. *Biophys. J.* **1990**, *57*, 260.
(54) Uesawa, Y.; Sugiura, Y. *Biochemistry* **1991**, *30*, 9242–9246.
(55) Lu, M.; Guo, Q.; Krishnan, B.; Golik, J.; Rosenberg, I. E.; Doyle, T. W.; Kallenbach, N. R. *J. Biomol. Struct. Dyn.* **1991**, *9*, 285–298.
(56) Lu, M.; Guo, Q.; Kallenbach, N. R. *Crit. Rev. Biochem. Mol. Biol.* **1992**, *27*, 157–190.
(57) Christner, D. F.; Frank, B. L.; Kozarich, J. W.; Stubbe, J.; Golik, J.; Doyle, T. W.; Rosenberg, I. E.; Krishnan, B. *J. Am. Chem. Soc.* **1992**, *114*, 8763–8767.

Scheme I. Mechanism of Action for Esperamicin A_1 and Calicheamicin γ_1^I

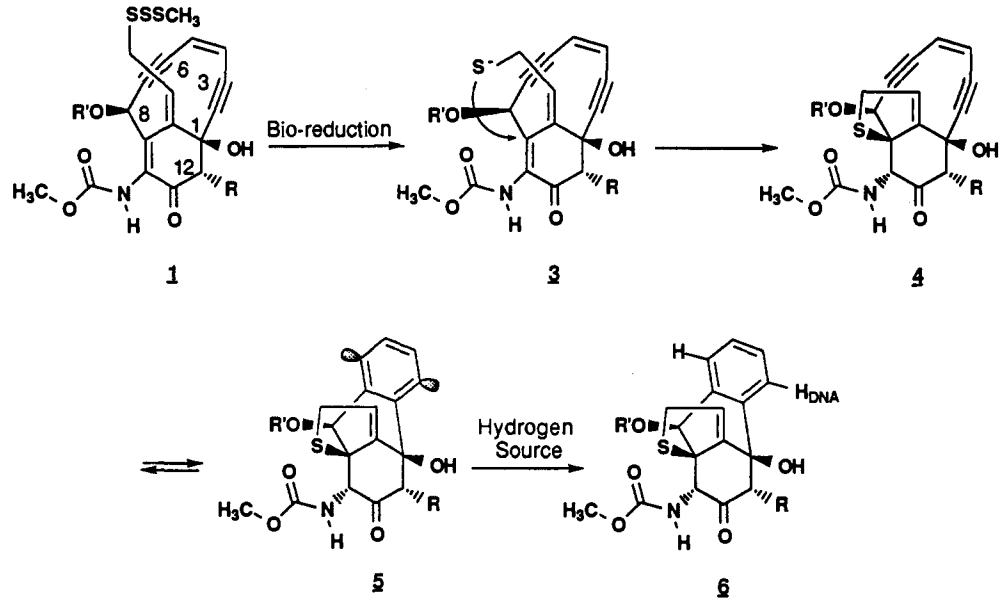

cleave DNA.[37-39,50-57] The focus of this work is the determination of the 3D structure of the DNA–esperamicin A_1 complex.

Background

Theoretical and synthetic studies on the cycloaromatization mechanism of several simple enediyne systems have predicted that the rate of cyclization is governed by the ring strain in the transition state.[59-63] Additionally, the theoretical studies,[60-63] using the semiempirical PRDDO-GVB method, predict that the CORE A-ring adopts a chair conformation prior to the transition state and that the transition state occurs via a least-motion closure pathway while developing 35% diradical character. The geometry of the enediyne system in the diradical transition state is planar, and the bond angles and lengths are more closely related to the cycloaromatized product of the Bergman reaction than the reactant.

A number of studies have focused on esperamicin's ability to cleave DNA. These studies have shown that esperamicin and its degradation products have weak absolute cleavage sequence specificity. However, they do have a preference for cleaving within 5′-Py Py tracks.[37-39,50-57] They have also shown that a given cleavage site is often accompanied by a cleavage site on the opposite strand, which is staggered by three base pairs in the 3′-direction, indicating that the diradical is being generated within the minor groove[64] of the DNA. This is supported by the fact that minor groove binding drugs inhibit esperamicin's ability to cause DNA strand breaks.[39] Furthermore, it has been shown that esperamicin A_1 causes single strand breaks by abstracting a C5*-hydrogen from the DNA backbone, while esperamicin C, like calicheamicin,[40-49] causes mostly double-stranded DNA breaks by abstracting a C5*-hydrogen from one strand of the DNA and a C4*-hydrogen from the opposite strand.[52,57] On the basis of analogy with calicheamicin,[40-49] it has been proposed [52,57] that the radical at C6 of esperamicin A_1 and C abstracts a C5*-hydrogen and the radical at C3 of esperamicin C abstracts the C4*-DNA hydrogen. Self-quenching of the C3 radical has been suggested[52] to explain why esperamicin A_1 causes only single DNA strand breaks. The self-quenching hypothesis was supported by CPK modeling studies which suggest that the deoxyfucose–anthranilate moiety can be proximal to the C3 radical.

There is very little direct structural information on the esperamicin–DNA complex. However, there are three studies on the structure of esperamicin and calicheamicin that must be considered. The X-ray crystal structure of the degradation product of dihydrocalicheamicin pseudoaglycon[11] provides important information about the conformations of the hydroxyamino and thiomethyl sugar rings and the relative geometry between them. Solution studies on calicheamicin ϵ, using COSY and ROESY techniques, have been conducted in three different solvents and over a temperature range of −50 to +50 °C.[65,66] This study suggests that the oligosaccharide is substantially preorganized and relatively rigid. Examination of the oligosaccharide portion of the X-ray structure and the NOE data suggests a strong similarity between the solution and X-ray structures. Additionally, the X-ray structure for esperamicin X has been determined,[34] providing us with information on the conformation of the cycloaromatized CORE, the deoxyfucose and anthranilate moieties, and their geometric arrangement relative to one another.

Reaction of Esperamicin A_1 with CT-DNA

Esperamicin A_1 (**1**) and calicheamicin γ_1^I share a common mechanism of activation. Both are converted into DNA-cleaving molecules in a four-step reaction sequence[27] (Scheme I), namely (1) reductive cleavage of the allylic methyl trisulfide; (2) Michael addition of the resulting thiolate (**3**) to the β-position of the enone (concomitantly forming the dihydrothiophene ring (**4**) while removing the bridgehead double bond); (3) aromatization of the enediyne to an aryl diradical (esperamicin R, **5**), and (4) hydr ogen abstraction from the environment (DNA, the drug itself, or solvent) to quench the diradical, producing esperamicin Z or calicheamicin ϵ (**6**).

The mechanism of DNA cleavage by the enediyne antibiotics neocarzinostatin[2-9] and calicheamicin[47] has been studied in *in vitro* systems. For example, calicheamicin, the closest structural analog of esperamicin A_1, aromatized in the presence of calf thymus DNA and methylthioglycolate to produce calicheamicin

(58) Doyle, T. W.; Golik, J.; Wong, H.; Lam, K. S.; Langley, D. R.; Forenza, S.; Vyas, D. M.; Kelley, S. Esperamicln A1 (BMY-28175) – A Novel, Antitumor Agent of the Diyne-ene Class. In *Cytotoxic Anticancer Drugs: Models and Concepts for Drug Discovery and Development*; Valeriote, F. A., Corbett, T. H., Baker, L. H., Eds.; Kluwer Academic Publlshers: Norwell, MA, 1992; p 345.
(59) Nicolaou, K. C.; Zuccarello, G.; Ogawa, Y.; Schweiger, E. J.; Kumazawa, T. *J. Am. Chem. Soc.* **1988**, *110*, 4866–4868.
(60) Snyder, J. P. *J. Am. Chem. Soc.* **1989**, *111*, 7630–7632.
(61) Snyder, J. P.; Tipsword, G. E. *J. Am. Chem. Soc.* **1990**, *112*, 4040–4042.
(62) Magnus, P.; Fortt, S.; Pitterna, T.; Snyder, J. P. *J. Am. Chem. Soc.* **1990**, *112*, 4986–4987.
(63) Snyder, J. P. *J. Am. Chem. Soc.* **1990**, *112*, 5367–5369.
(64) Dervan, P. B. *Science* **1986**, *232*, 464–471.
(65) Walker, S.; Valentine, K. G.; Kahne, D. *J. Am. Chem. Soc.* **1990**, *112*, 6428–6429.
(66) Walker, S.; Yang, D.; Kahne, D. *J. Am. Chem. Soc.* **1991**, *113*, 4716–4717.

Scheme II

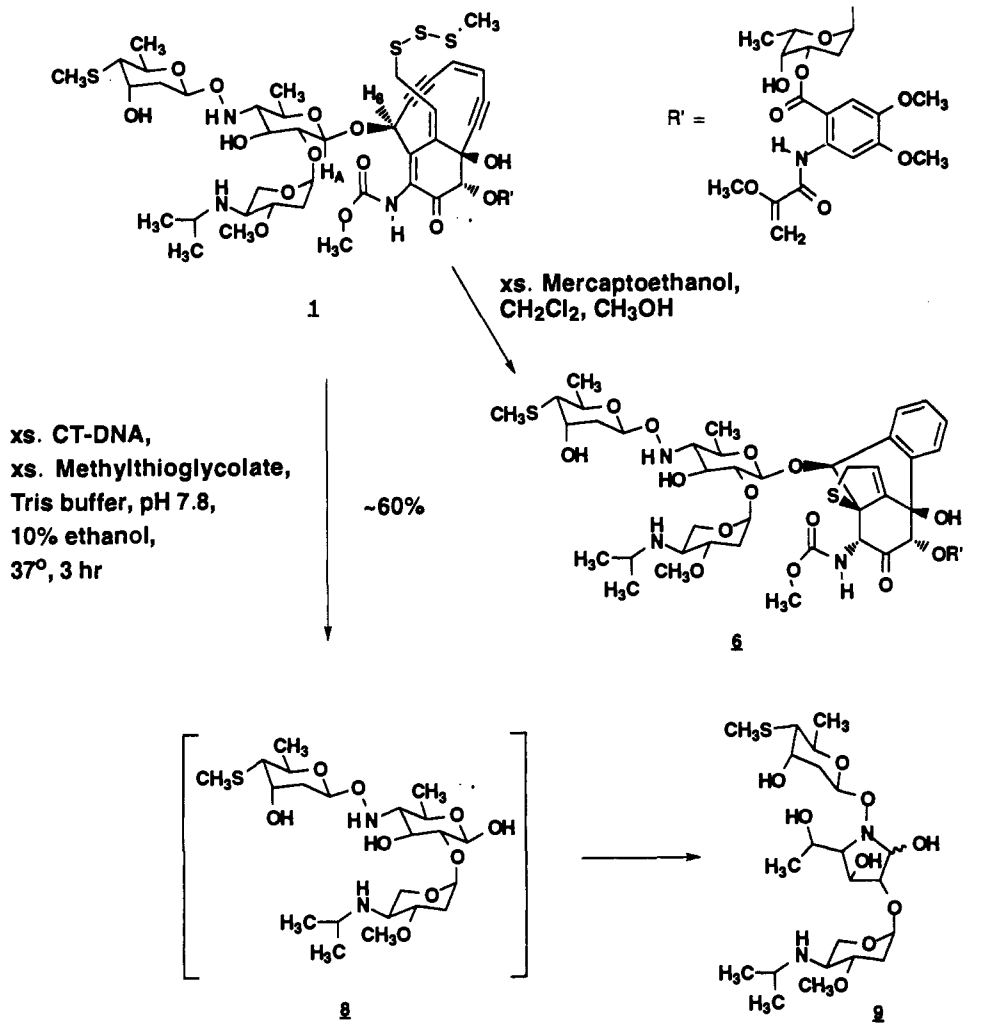

ϵ in 65% yield. It has been shown that the calicheamicin diradical intermediate abstracts hydrogen atoms almost exclusively from the carbohydrate backbone of the DNA, suggesting that DNA may serve as a catalytic template for quenching the diradical intermediate.[42,48,67].

Interestingly, esperamicin A_1 produced no detectable quantity of esperamicin Z under analogous reaction conditions with CT-DNA. Instead, the cleavage of the glycosidic bond at the C8 position was observed (Scheme II). The major esperamicin product from this reaction is the rearranged trisaccharide fragment (**9**) which was isolated in 60% yield. We have previously observed the cleavage of the trisaccharide fragment from esperamicin A_1 following its reduction with sodium borohydride.[33] It should be noted that the trisacchardie fragment undergoes spontaneous rearrangement of the pyranose form of the hydroxyamino sugar (**8**) to its furanose carbinolamine equivalent (**9**). Traces of the aromatized CORE were detected in the ^{1}H-NMR spectra of the crude reaction mixtures; however, the aromatized CORE fragment has never been isolated and completely characterized.

The base sensitivity of both esperamicin A_1[33] and calicheamicin γ_1^I [13] has been demonstrated but appears inadequate to explain the differences observed between the reaction of esperamicin A_1 and calicheamicin γ_1^I with CT-DNA under analogous reaction conditions. Additionally, when the reaction between esperamicin A_1 and CT-DNA was repeated at lower pH (7.0, 7.2, and 7.4), only minor variations in the yield of the rearranged trisaccharide fragment (**9**) were observed.

The mechanism by which the cleavage of the C8 glycosidic bond occurs has remained clouded due to the fact that the product-(s) related to the CORE have not been isolated and the role that the individual radicals play is unknown.

Figure 3. Oligonucleotide used in the affinity cleavage and osmium tetraoxide experiments.[55,68] The arrows mark the strong esperamicin A_1 cleavage sites. The dots mark the sites that were protected by esperamicin A_1 during OsO_4 oxidation. The 10 base pair sequence in bold type was used in this modeling study.

Footprinting of Bound Esperamicins A_1 and C[68]

Features of the groove structure in duplex DNA can be monitored by use of the reactive probe osmium tetraoxide (OsO_4).[69] OsO_4 oxidizes the thymine C5–C6 double bond, which lies in the major groove, preferentially in the open rather than the base paired state. Unactivated esperamicin A_1 when bound with DNA reduces the ability of OsO_4 to oxidize thymine residues, when compared to the oxidation of naked DNA (Figure 3). In contrast, the oxidation of the unactivated DNA–esperamicin C complex produced oxidation levels comparable to that of naked DNA. Esperamicin C is an analog of esperamicin A_1 which lacks the deoxyfucose and anthranilate residues.[28,37] This suggests that the groove structure of the DNA–esperamicin A_1 complex

(67) Warpehoski, M. A.; Hurley, L. H. *Chem. Res. Toxicol.* **1988**, *1*, 315–333.

(68) Lu, M.; Guo, Q.; Kallenbach, N. R. Personal communication.
(69) Lilley, D. M. J.; Palecek, E. *EMBO J.* **1984**, *3*, 1187–1192.

is close to that of regular B-DNA[69] and possibly that at least a portion of the deoxyfucose and/or anthranilate moieties are bound in the major groove.

Goals and Limitations

The goal of this work is to develop a dynamical model of the DNA–esperamicin complex that is consistent with *all* of the available experimental data. The resultant model will be used to gain insights into the mechanism of DNA cleavage by esperamicin A_1, specifically its mode of binding to DNA and what the individual residues contribute to the drug's ability to bind with and cleave DNA. Additionally, the fate of the radical centers will be examined to determine which is responsible for cleaving the DNA and whether the unproductive radical can participate in the homolytic cleavage of esperamicin. Finally, the DNA pattern and sequence specificity of cleavage exhibited by esperamicin will be explored.

It is important to keep in mind that only a droplet of solvent (water) encases the DNA–drug complex and that counterions are not included in the model. As a result, the shape, volume, and pressure of the droplet system may not remain constant, since they are maintained only by the hydrostatic nature of bulk water. Furthermore, the calculations rely on an assumed force field and our chemical intuition to correctly use the force field. One of the more difficult problems in force field calculations is correctly dealing with the long-range nonbonded interaction. Since it is not possible to calculate all possible nonbonded interactions, at least with today's computational power, one must use a smoothing function to force these long-range interactions to go to zero at some distance.[70] Due to these limitations, it is important to have good experimental data which can be used as a guide in model building and as a reference to verify that the calculations are proceeding in the right direction.

Criteria Used to Validate the Model

From the DNA-nicking and cleavage affinity studies,[39,50-57] we have learned that esperamicin A_1 predominantly causes single strand breaks, that at least part of the molecule binds in the minor groove of DNA, that it has a preferred cleavage sequence specificity of 5′-Py Py, and that either the 5*- or 5**-hydrogen of the deoxyribose is abstracted. From the PRDDO-GVB studies,[60] we know that the geometry of the diradical transition state is much more benzene-like; i.e., the bond angles for the acetylene atoms are much closer to 120° than 180°. On the basis of the above experimental and theoretical observations, the following criterion was used in model building and validation of the model. A model of the DNA–esperamicin complex should place at least a portion of the drug in the minor groove of the DNA in a way that positions C3 or C6 (the esperamicin carbons that carry the radicals in the transition state) of the drug near either a H5* or H5** of the cleaved Py base. The theoretical studies suggest that a model between 3,6-dehydroesperamicin Z (**5**, esperamicin R) and DNA should be better than a DNA–esperamicin A_1 model at predicting the conformation of the complex that leads to DNA cleavage, since esperamicin R more closely mimics the diradical transition state.

The benzene carbon–hydrogen bond can be described by the vector that extends through any two para–carbons; i.e., the C1–C4–C4H angle is 180°. Assuming that the 1,4-diradical has a geometry similar to that of a benzene hydrogen, a DNA hydrogen that lies along the benzene carbon–hydrogen vector would be aligned with the radical orbital. Given two hydrogens of approximately equal distance from the carbon-centered radical, the one aligned most closely with the axis of the radical orbital would be abstracted.[16,71] Therefore, the criterion used in selecting the most likely hydrogen candidate for abstraction is based on distance and angle. The closest hydrogen atoms to C3 or C6 are candidates if they are near or on the line extending through the radical-centered carbons C3 and C6 (C3–C6–(DNA)H or C6–C3–(DNA)H angle of 180°); if two hydrogen atoms are nearly equal in distance from C3 or C6, then the one that is the closest to the 180° angle is selected.

Calculations

Computational Details. The modeling studies were conducted with Polygen's[72] Quanta/CHARMM software (version 3.1) and force field[73-75] running on an IBM Risk 6000/540 workstation. The oligonucleotide and the drug were treated as electrically screened charged systems. The phosphate and ammonium were screened to –0.32 and +0.32, respectively, according to Manning counterion condensation theory,[76] and a continuous dielectric of one was used. The switch/vswitch functions were used in both the energy minimization (EM) and molecular dynamics (MD) for the nonbonded, van der Waals, and electrostatic interactions between 9.5–10.5 Å with an 11.50-Å cut list.[77,78] In parallel studies, the shift/vshift functions were used to smooth long-range interaction to zero at 9.0 and 14.0 Å with 10.0- and 15.0-Å cut lists,[70] respectively. In several of the runs, the CHARMM hydrogen bond potential was used. A switching function was used to smooth the potential to zero between 4.0 and 5.0 Å and 130 and 110° with a cut list of 5.5 Å and 90°, respectively. The Verlet algorithm[79] was used to calculate the classical equations of motion for the atoms, and the X–H bonds were fixed using the SHAKE algorithm[80] during MD.

All in-vacuum calculations were performed without cutoffs using a distance-dependent dielectric.

All EM studies were minimized to a RMS gradient force of ≤0.100 with either a steepest descent (SD)[81] or an adopted-basis Newton–Raphson (ABNR) minimizer[82] unless otherwise stated.

The following CHARMM detailed dynamics prescription[16] was used throughout this study. In a 1.5-ps heating phase, the temperature was raised to 300 K in steps of 10 K over 0.05-ps blocks. The MD velocities were reassigned after every step on the basis of the Gaussian approximation to the Maxwell–Boltzmann distribution. This was followed by an equilibration phase in which the velocities were allowed to rescale over the next 13.5 ps in steps of 0.25 ps to stabilize the system within a 300 ± 5 K window. The production phase continued for another 125–300 ps where the velocities were allowed to rescale every 0.5 ps to keep the system within a 300 ± 5 K window.

Model Building. The d(CGCAATCCTG)·d(CAGGATTGCG)[83] oligonucleotide was constructed using Quanta's nucleic acid builder. The geometries of the intercalation clefts from the d(CGTACG)–(daunomycin)$_2$[84] (perpendicular intercalator) and d(CG)–proflavine[85] (parallel intercalator) crystal complexes were inserted into separate oligonucleotides, at the 5′-ApA/3′-TpT step, to explore the possibility of an intercalation mode of binding. The oligonucleotide was minimized in a vacuum with 50 steps of SD minimization to locate a local minimum in

(70) Loncharich, R. J.; Brooks, B. R. *Proteins: Struct., Funct., Genet.* **1989**, *6*, 32–45.
(71) Hawley, R. C.; Kiessling, L. L.; Schrieber, S. L. *Proc. Natl. Acad. Sci. U.S.A.* **1989**, *86*, 1105–1109.
(72) Polygen Corp., 2000 Fifth Avenue, Waltham, MA 02254.
(73) Momany, F. A.; Rone, R. *J. Comput. Chem.* **1992**, *13*, 888–900.
(74) Momany, F. A.; Rone, R. Personal communication.
(75) *QUANTA Parameter Handbook*, Release 3.0; Polygen Corporation: Waltham, MA, 1990; p 4.
(76) Manning, G. S. *Q. Rev. Biophys.* **1978**, *11*, 179–246.
(77) Nilsson, L.; Karplus, M. *J. Comput. Chem.* **1986**, *7*, 591–616.
(78) Tidor, B.; Irikura, K. K.; Brooks, B. R.; Karplus, M. *J. Biomol. Struct. Dyn.* **1983**, *1*, 231–252.
(79) Verlet, L. *Phys. Rev.* **1967**, *159*, 98–105.
(80) Ryckaert, J. P.; Cicotti, G.; Berendsen, H. J. C. *J. Comput. Phys.* **1977**, *23*, 327–341.
(81) Levitt, M.; Lifson, S. *J. Mol. Biol.* **1969**, *46*, 269.
(82) Brooks, B. R.; Bruccoleri, R. E.; Olafson, B. D.; States, D. J.; Swaminathan, S.; Karplus, M. *J. Comput. Chem.* **1983**, *4*, 187–217.
(83) See Figures 3A, 1, and 4 from ref 55.
(84) Wang, A. H.-J.; Ughetto, G.; Quigley, G. J.; Rich, A. *Biochemistry* **1987**, *26*, 1152–1163.
(85) Shieh, H. S.; Berman, H. M.; Dabrow, M.; Neidle, S. *Nucleic Acids Res.* **1980**, *8*, 85.

the vicinity of the starting structure. The minimized structure was then used in the DNA–esperamicin docking studies.

The six residues that make up esperamicin Z were constructed in Chemnote and assembled in the molecular editor of Quanta. The atomic charges were assigned on the basis of Quanta's fragment library and smoothed to neutrality over all nonpolar atoms. The charges of the ammonium groups were then adjusted to give an overall charge of +0.32. The hydrogens at C3 and C6 were omitted by using the C6R CHARMM atom type, to more closely mimic the diradical form of esperamicin.

The diradical form of esperamicin Z (**5**, esperamicin R) was then docked with the DNA in a way that positioned C3 and C6 near C5* of thymine 17 (T:17) and cytosine 8 (C:8), respectively. The continuous-energy facility in Quanta was used in the docking procedure to find the optimal starting point for EM. The DNA was constrained, and the complex was minimized with 50 steps of ABNR minimization, followed by 50 steps of unconstrained SD minimization prior to solvation.

The DNA–drug 10-mer complex consisting of 20 nucleic acid residues and six esperamicin R residues was solvated in a droplet of water containing 824 preequilibrated TIPS3 water molecules. This was accomplished by placing the center of mass of a residue in the center of a 10 Å sphere containing pre-equilibrated TIPS3 waters. Then all water molecules whose oxygen was within 2.3 Å of another solvent or solute heavy atom (non-hydrogen atom) were removed. The solute was constrained, and the system was minimized with 200 steps of SD followed by 1000 steps of ABNR minimization. The constraints were removed, and the system was minimized with an additional 200 steps of SD followed by 1000 steps of ABNR. This minimized system was then used as the starting point for MD using the protocol described above.

Analysis. The Curves, Dials, and Windows (CDW) analysis package introduced by Ravishanker et al.[86] was used to analyze the MD results in terms of a full set of conformational and helicoidal parameters. The time evolution of the conformational and helicoidal parameters was followed in the analysis, providing a complete description of the dynamical model obtained in the simulation. The structural inferences described below are based on this analysis. A complete CDW graphical description of all the DNA parameters is available in the supplementary material.

Drug Docking Studies

In constructing the DNA–esperamicin 10-mer model several modes of binding were considered. Our first bias was to stretch esperamicin along the minor groove of the DNA. This was done by placing the thiomethyl and hydroxyamino sugars, CORE, deoxyfucose, and anthranilate in the minor groove. The isopropylamino sugar was placed on the lip of the minor groove so that the ammonium group could form a salt bridge with the phosphate backbone. Several problems became immediately apparent with this model. The radical-bearing carbons (C3 and C6) are pointed along the minor groove close to and directionally aligned for a C4*-DNA hydrogen abstraction from each strand of the DNA. Esperamicin was also modeled as an intercalator by inserting of the anthranilate moiety between the DNA base pairs of the 5′-ApA/3′-TpT step. The remainder of the drug was stretched along the minor groove of the DNA as described above. The anthranilate moiety was intercalated into the binding cleft either by placing its aromatic ring between T:16 and T:17 on the lower strand or by rotating 180° about the $C7^{iv}$–$C8^{iv}$ bond to place it near the A:4 and A:5 side of the cleft. In both modes of intercalation, the long axis of the anthranilate is approximately parallel with the long axis of the DNA base pairs. Of the four different intercalation models, only the mode which placed the aromatic ring of the anthranilate near the upper strand of the intercalation cleft, based on the d(CG)–proflavine cleft geometry, produced a model that correctly predicted the abstraction of a C5*-hydrogen. This model places the radicals at C3 and C6 close to and directionally aligned to abstract the H1* of T:17 and the H5* of C:8, respectively. Finally, esperamicin was modeled as a simultaneous minor–major groove binder (Figure 4 (top left)). The model was generated by modifying the minor groove binding model. The placement of the trisaccharide (thiomethyl, hydroxyamino, and isopropylamino sugars) with respect to the DNA was unchanged; however, by simply rotating about the bonds of the glycosidic linkage between the CORE and hydroxyamino sugar, the radicals at C3 and C6 can be placed near and directionally aligned to abstract a DNA-hydrogen from C5* of T:17 and C:8, respectively. In the solvated energy-minimized minor–major groove complex, the thiomethyl sugar lies in the minor groove sandwiched between the DNA backbones where its 3″-axial hydroxyl group forms a hydrogen bond with N3 of G:14. The hydroxyamino sugar unexpectedly lies flat in the mouth of the minor groove. The hydroxyl at C3′ hydrogen bonds with O2P of T:9, and C6′ is positioned near C4* and C5* of the deoxyribose of T:16. The bound geometry of these two sugars relative to one another is very similar to that found in the crystalline environment;[11] i.e., their planes, defined by C2, C3, C5, and O5, are approximately perpendicular to one another. The isopropylamino sugar ring sits within van der Waals (VDW) contact over the deoxyribose of C:8, and its ammonium group at C4‴ forms a salt bridge with O1P of T:9. The CORE occupies the space in the minor groove approximately equally distant between C5* of C:8 and T:17, and the tertiary hydroxyl at the C1 hydrogen bonds with O3* of T:16. The bulky deoxyfucose group and sterochemistry at C:12 force the diradical-containing ring to point into and slightly down the minor groove (in the 3′-direction relative to C5* of T:17 and away from the trisaccharide group). The deoxyfucose forms a bridge across the DNA backbone between the CORE in the minor groove and the anthranilate moiety in the major groove. The deoxyfucose resides over the deoxyribose of T:17 between the two phosphate groups of T:17 and G:18. The anthranilate moiety lies to one side of the major groove, interacting predominantly with the major groove side of the DNA backbone. The pyruvate group sits within 3.5–4.0 Å of the T:17 C5-methyl and hydrogen bonds with O1P of T:17 via its amide hydrogen. At the other end of the anthranilate, the methoxy group at $C11^{iv}$ accepts a hydrogen bond from the 4-amino group of C:19 and the methoxy group at $C10^{iv}$ is approximately 3.15 Å from C2* of G:18. The anthranilate aromatic ring hovers over G:18. The hydrogens at C8 of G:18 and C2* of T:17 are within the anthranilate shielding cone. The only problem with the energy-minimized intercalation and minor–major groove models is that they protray esperamicin A_1 as a double strand cleaving molecule that produces cut sites that are staggered by four base pairs in the 3′-direction. While esperamicin has been shown to produce strong cuts at both of these sites (Figure 3),[83] these cuts presumably occur via different molecules as esperamicin causes predoimately single strand breaks. Since we have no direct experimental data available to assign which radical is responsible for causing the cleavage site, we chose to let the MD decide. All of the energy-minimized models described above were subjected to both in-vacuum and solvated MD for 100 ps or more. None of the in-vacuum simulations produced stable MD runs that were consistent with the available experimental data, suggesting the importance of structural water molecules for stabilizing the DNA–esperamicin complex. Of the solvated models, only the minor–major groove binding model provided a stable MD simulation that was consistent with all of the known experimental data and correctly predicted the abstraction of a C5*-hydrogen using the criteria described above. This model was used as the starting point for the MD studies described below.

Evaluation of Long-Range Smoothing Functions

The minor–major groove model was subjected to the MD protocols described above using either the switch/vswitch or shift/vshift long-range nonbonded smoothing functions. The simu-

(86) Ravishanker, G.; Swaminathan, S.; Beveridge, D. L.; Lavery, R.; Sklenar, H. *J. Biomol. Struct. Dyn.* **1989**, *6*, 669–699.

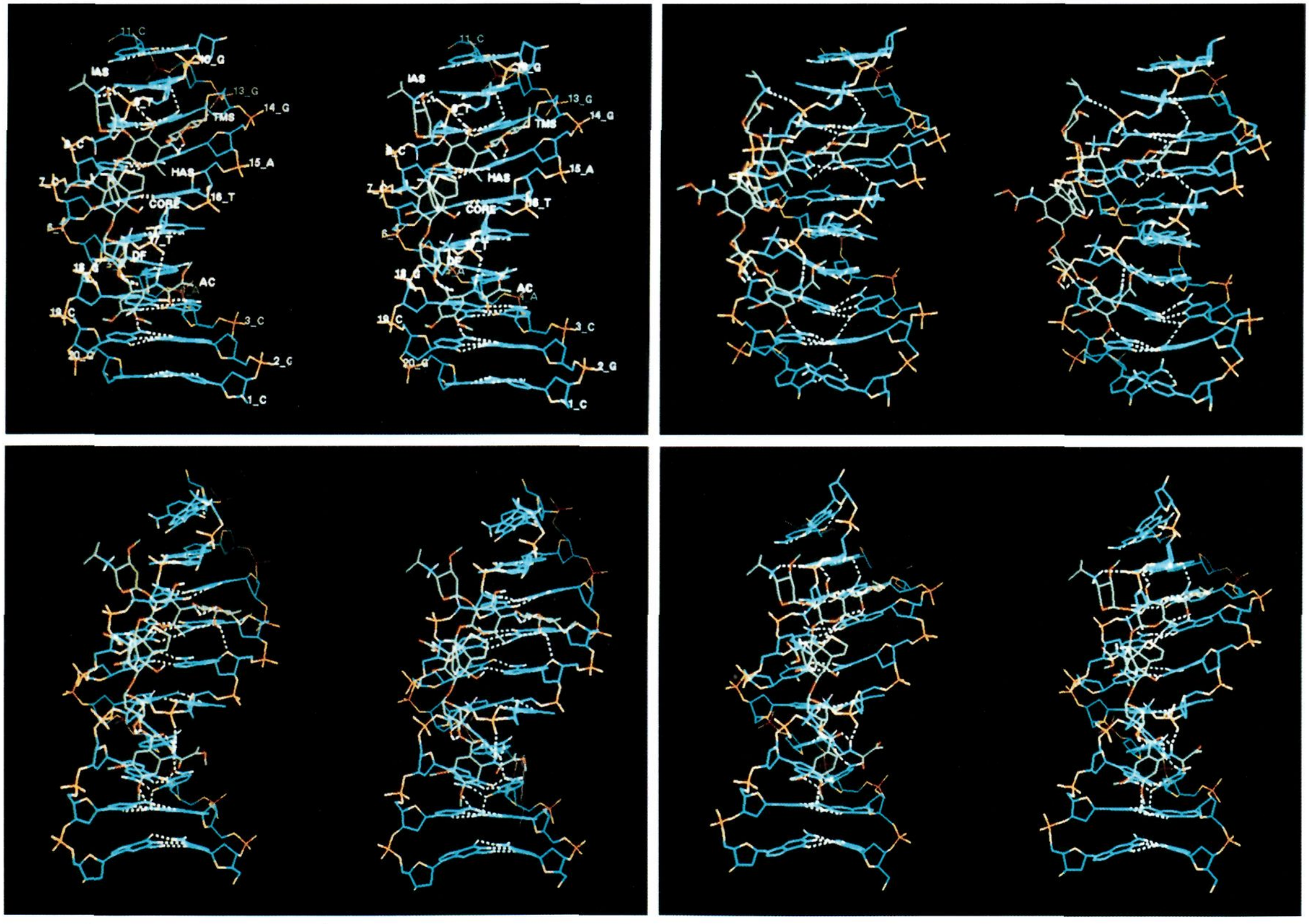

Figure 4. Stereoviews: (top left) Energy-minimized complex between esperamicin R and d(CGCAATCCTG)·(CAGGATTGCG) duplex oligonucleotide. (top right) Snapshot of the 90-ps frame from the dynamics amination. (bottom left) Snapshot of the 240-ps frame. (bottom right) Snapshot of the 315-ps frame. The coloring scheme for the DNA is blue for carbon, light green for nitrogen, yellow for oxygen, and amber for phosphate. The coloring scheme for esperamicin is green for carbon, red for oxygen, blue for nitrogen, and yellow for sulfur. All polar hydrogens are white. Nonpolar hydrogens were omitted for the sake of clarity. The DNA C:8 C5*-hydrogens and T:17 C5*-hydrogens as well as esperamicin C6 and C3, upper and lower, respectively, are purple. The white dotted lines depict hydrogen bonds.

lations in which the switch/vswitch smoothing function was used were found to be extremely stable with a maximum RMS deviation of less than 0.7 Å from the starting point. An examination of the calculated temperature factors revealed that they were 10–100 times lower than would be expected on the basis of comparison with drug–DNA crystal structures.[87,88] Though the results from the switched MD runs seem very reasonable in light of the experimental data, the low RMS deviation from the starting point and temperature factors suggests that the simulation is trapped in a very deep and narrow potential well and that the complex is profoundly rigid or that flaws exist in the switched protocol. The shifted MD runs produced stable simulations with a maximum RMS deviation of 2.5 Å from the starting structure. The calculated temperature factors were found to be slightly higher (1–3 times) than that found in DNA–drug crystal structures. This seems reasonable, since solution structures are not influenced by crystal-packing forces. One would expect them to have fluctuations that are equal to or slightly higher than their crystal counterparts. The shifted MD simulations produced DNA structures whose strands were loosely held together. Examination of the CDW[86] analysis for the DNA revealed that the sugars continuously repucker throughout the simulations, the most noticeable deviations away from classical B-DNA are the intra-base pair propeller twist parameter and a slight widening of the minor groove. In the simulation with the 14-Å cutoff, the average propeller twist for individual base pairs varied from –2.8° to –62.0° with an average for all base pairs of –28.02° compared to 3.7° and 13.7° for canonical B-DNA and A-DNA, respectively. This was predominantly due to an excessive amount of inter-base pair hydrogen bonding. The average interstrand phosphate distance fluctuated about 12.8 Å (center of mass to center of mass) compared to the closest interstrand phosphate distance in canonical B-DNA of 11.5 Å.[89] The largest deviations in the minor groove width occured on the ends and along the drug-binding site. Nonetheless, the DNA maintained its B-DNA character as denoted by the inter-base pair parameters rise and twist angle, and axis–base parameters X-displacement (XDP) and inclination (INC). Additionally, the average intrastrand phosphate distance fluctuated around 6.6 Å, consistent with canonical B-DNA. In the 9.0-Å cutoff simulation, many of the same problems were observed as well as local base pair melting. Many of the inter-base pair hydrogen bonds observed in these simulations were very poorly aligned, i.e., away from the ideal N–H···O hydrogen bond angle of ~180° and the ideal H···O=C hydrogen bond angle of ~120°. By implementing the CHARMM hydrogen bond potential as described above, the correctly aligned hydrogen bonds will have more weight in determining the conformation that the poorly aligned ones. The potential had its most profound effect on the 9.0-Å cutoff simulation by eliminating the local base pair melting and slightly reducing the number of inter-base pair hydrogen bonds in all the shifted MD simulations. Not unexpectedly, the incorporation of the hydrogen bond potential into the calculation caused the DNA to stiffen slightly. This only slightly reduced the calculated temperature factors and caused the sugar repuckering to settle down somewhat. Using the hydrogen bond potential with the 9.0-Å cutoff produced results that are qualitatively the same as the 14-Å cutoff run in less than half the CUP time. Due to the computational expense of the longer cutoff, only the run with the 9.0-Å cutoff and hydrogen bond potential was extended past 140 ps to 315 ps. The 315-ps run will be used for the discussion that follows.

Dynamical Model of the DNA-Drug Complex

The greatest changes occurred in the complex at the onset of the dynamics, demonstrating how easy it is to get trapped in a local minima using energy-minimization techniques.[16,90,91] Throughout the first 65 ps of the dynamics trajectory, the DNA–drug complex underwent a steady gradual change. However, most of the individual DNA conformational and helicoidal parameters stabilized by the end of the equilibration phase of the calculation. Some of the more significant DNA helicoidal parameters are XDP, INC, rise, twist, and propeller, as they are the most indicative of A- or B-form DNA. All of these helicoidal parameters were found to stabilize near to B-DNA and away from A-DNA values, placing the DNA of this DNA–drug complex firmly in the B-DNA family. However, as noted above, the propeller twist for almost all of the base pairs is abnormally large and negative with one noteworthy exception, the G:2–C:19 propeller twist stabilized around 14.8°, which is very close to the 13.7° value of canonical A-DNA. The DNA conformational parameters remained quite active throughout the entire simulation. The sugar puckers were found to be highly mobile, repuckering between $C_{2'\text{-endo}}$, $C_{1'\text{-exo}}$, and $C_{4'\text{-exo}}$ with an occasional visit to $C_{3'\text{-endo}}$. Several crankshaft transitions were observed at C:3, C:7, T:9, and G:14. Over the first 65 ps, esperamicin R crept down the minor groove in the 5′-direction relative to the phosphate group of T:9. This slight movement of esperamicin R coupled with a crankshaft transition (15–16 ps) about the α- and γ-DNA conformational parameters between C:7 and C:8 moved the closest C5* hydrogen of C:8 to greater than 4 Å away from the C6 radical, while the distances and alignments between the C5* hydrogens of T:17 and the radical at C3 remained virtually unchanged. From this new binding position (Figure 4 top right), the hydrogen bonding network between the drug and the DNA remained intact with one exception. The thiomethyl sugar residue moved away from the floor of the minor groove and slightly in the 3′-direction relative to G:14, where it hydrogen bonds intermittently with O4* or O3* of A:15 via its 3″-axial hydroxyl group. For the next 100 ps (65–165 ps), the complex remained quite stable with the exception of a noticeable drift in the inter-base pair buckle parameter toward values that are more in line with canonical B-DNA. The base pair buckle remained relatively constant and near the energy-minimized value for the first 65 ps. For the first 65 ps, these values ranged from a low of –20.3° to a high of 26.1° and drifted to values of –6.8° to 19.3° by the end of 165 ps compared to 0.2° for canonical B-DNA. Over the next 20–25 ps (165–190 ps), several of the inter-base pair hydrogen bonds disappeared and the propeller twist for these base pairs decreased and stabilized. The decrease in the propeller twist for the C:7–G:14 base pair moved the 2-amino group of G:14 closer to the hydroxyl group of the thiomethyl sugar (Figure 4 (bottom left)). This started a three-way hydrogen bonding tug of war between the 2-amino group of G:14 (donor), N3 of G:14 (acceptor) and O4* of A:15 (acceptor), and the hydroxyl group of the thiomethyl sugar (acceptor/donor) that lasted for the better part of the next 100 ps (190–315 ps). The propeller twist for the A:3–T:17 base pair increased, bringing the methyl group of T:17 in close VDW contact with the anthranilate residue. Over this same time period (165–190 ps), the ammonium group of the isopropylamino sugar residue drifted away from the phosphate group of T:9 and stabilized midway between the phosphate groups of C:8 and T:9. Its aliphatic ring remained within VDW contact with the deoxyribose group of C:8. Again the dynamical structure stabilized. The DNA remained stable throughout the remainder of the simulation (190–315 ps). In the last 35–40 ps of the run, G:14 won the tug of war and the thiomethyl sugar residue was pulled deeper into the minor groove and closer to the deoxyribose of T:9 and the isopropylamino sugar ammonium group returned to hydrogen bond with the phosphate group of T:9 (Figure 4 (bottom right)). It is interesting to note that during the course

(87) Wang, A. W.-J.; Nathans, J.; van der Marel, G.; van Boom, J. H.; Rich, A. *Nature* **1978**, *276*, 471–474.
(88) Kopka, M. L.; Yoon, C.; Goodsell, D.; Pjura, P.; Dlcerson, R. E. *Proc. Natl. Acad. Sci. U.S.A.* **1985**, *82*, 1376–1380.
(89) Saenger, W. *Principles of Nucleic Acid Structure*; Speinger-Verlag: New York, 1984; p 226.
(90) Kirkpatrick, S.; Gelatt, C. D.; Vecchi, M. P. *Science* **1983**, *220*, 671–680.
(91) Brunger, A. T.; Clore, G. M.; Gronenborn, A. M.; Karplus, M. *Proc. Natl. Acad. Sci. U.S.A.* **1986**, *83*, 3801–3805.

Scheme III

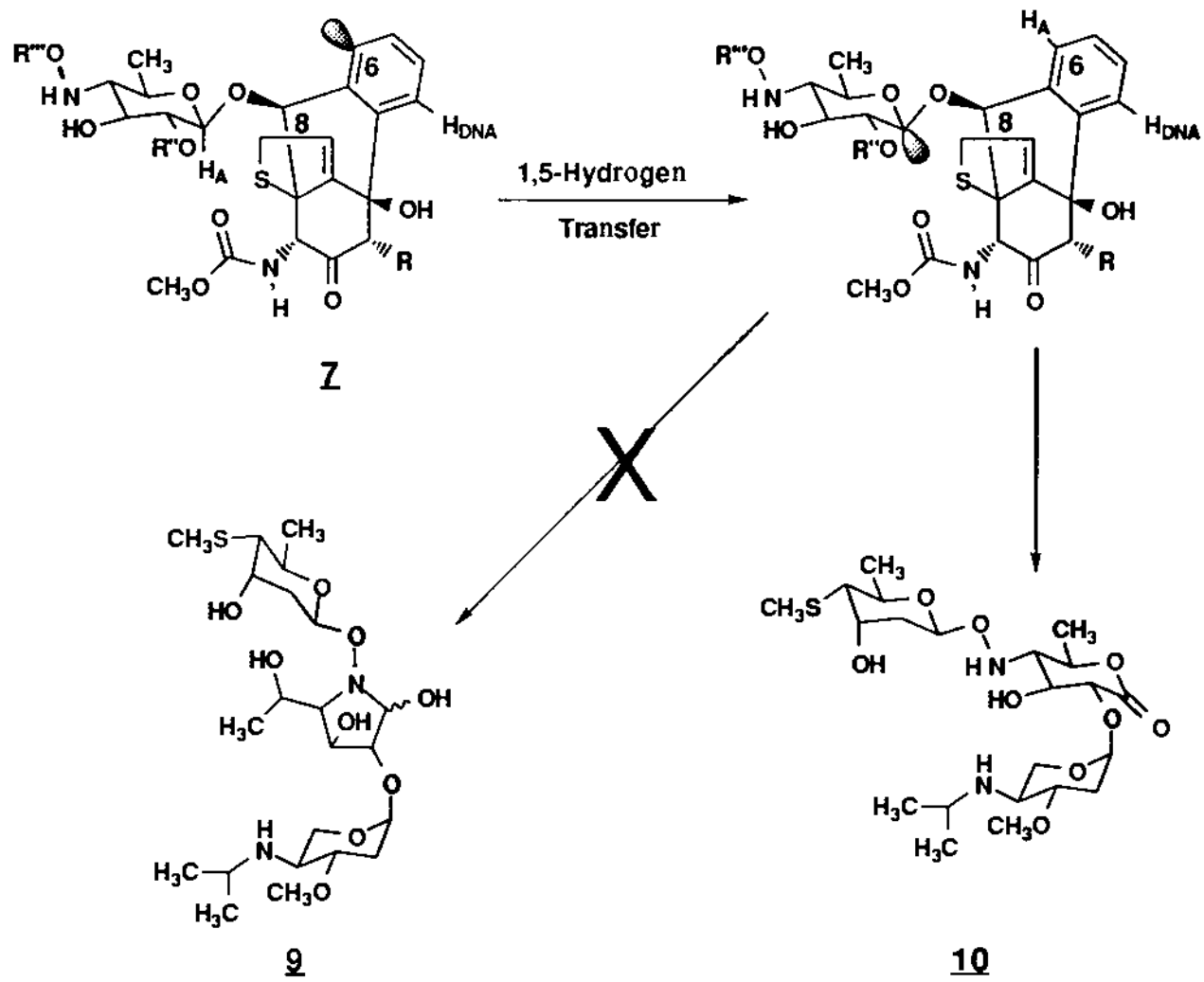

Table 1

		5′-	(–B4	–B3	–B2	–B1	C1	B1	B2)	-3′
A[a]										
	11	12	13	14	15	16	17	18	19	20
5′-	C	A	G	G	A	T	T	G	C	G
3′-	G	T	C	C	T	A	A	C	G	C
	10	9	8	7	6	5	4	3	2	1
B[b]										
		Pu	30	51	58	16	7	33	44	
		Py	37	16	9	51	60	34	23	
C[c]										
		A	14	29	26	10	4	18	21	
		G	16	22	32	6	3	15	23	
		C	20	10	2	21	26	16	11	
		T	17	6	7	30	34	18	12	

[a] The DNA sequence used in this study is aligned with the population analysis. The bold DNA bases make up the esperamicin binding site. One atom or more of the highlighted bases are ≤4.5 Å from esperamicin. Esperamicin makes direct contact with the floor of the minor and major grooves at the underlined and double underlined bases, respectively. Population analysis of the DNA bases within the 67 strong cut sites. [b] Base family, purine (Pu) or pyrimidine (Py). [c] Base type, adenine (A), guanine (G), cytosine (C), and thymine (T).

of the dynamics simulation esperamicin R has come full circle with respect to its hydrogen bonding pattern with its host DNA.

Esperamicin R makes direct contact with the floor of the minor groove at C:8 and G:14 and with the major groove floor at T:17, G:18, and C:19, based on a water-accessible surface analysis of the DNA (Table IA). Esperamicin's minor–major groove binding motif allows it to interact with more bases from the strand it cuts. A spine of hydration runs the length of the minor groove and rhythmically hydrogen bonds with every base with the exception of C:8 and G:14, where it is disrupted by the thiomethyl sugar residue. There are five to seven water molecules between the floor of the minor groove and esperamicin R. Several of these water molecules periodically hydrogen bond with and between (via a single water bridge) the CORE C1-hydroxyl and O5′ of the hydroxyamino sugar or the phosphate group of T:17 and appear to play a structural role in the DNA–drug complex.

During the course of this simulation the carbon-bearing radical at C3 has remained close (Figure 5 (top)) to and directionally aligned (Figure 5 (bottom)) for abstraction of a C5*-hydrogen from T:17. On the basis of the distance criteria, the T:17 H5* and H5** are both candidates; however, the inclusion of the angle criteria favors the T:17 H5**. It should be noted that the abstraction of either the H5* or H5** is consistent with the available experimental data.

The fate of the radical at C6 is still unclear. Figure 5 shows the distance and angle of the closest DNA and esperamicin hydrogens with respect to C6. The DNA C5*-hydrogen can be ruled out on the basis of distance and experimental data (esperamicin causes predominantly single strand breaks). The average distances between C6 and the C1′ anomeric hydrogen (HA) and the C8 hydrogen (H8) are approximately equal. However, both the C3–C6–HA and C3–C6–H8 angles are much closer to 90° than to 180°, making these hydrogens barely suitable as candidates for abstraction.[92] The abstraction of HA by the C6 radical is effectively a 1,5 free-radical migration, while the H8 abstraction is a 1,3-migration. The 1,5-hydrogen transfers are very well-known,[93] as they can readily adopt a favorable transition-state geometry. However, direct 1,3 free-radical migrations are very rare and may not occur at all.[93] This is presumably due to the fact that the energetically most favored linear geometry for the C- -H- -C transition state is not obtainable.[92,93] In the DNA–esperamicin matrix, neither the 1,5- nor 1,3-hydrogen transfer can adopt the desired transition-state conformation. Additionally, if the 1,5-hydrogen transfer occurred, the lactone form of trisaccharide **10** (Scheme III) would be expected as a major product. This product has not been observed. Mechanistically the 1,3-hydrogen transfer from C8 (**7**, Scheme IV) to C6 (**11**) followed by oxidation to **12** and fragmentation of the glycosidic bond is analogous to the mechanism invoked for the cleavage of DNA via radical chemistry.[94,95] Opening of the resultant hemiacetal (**8**) to an aldehyde followed by ring closure via a Schiff base reaction with the hydroxyl amine would produce

(92) Huang, X. L.; Dannenberg, J. J. *J. Org. Chem.* **1991**, *56*, 5421–5424.
(93) March, J. Free-Radical Rearrangements. *Advanced Organic Chemistry*, 3rd ed.; J. Wiley & Sons: New York, 1985; pp 955–958.
(94) Kappan, L. S.; Goldberg, I. H. *Biochemistry* **1983**, *22*, 4872–4878.
(95) Kappen, L. S.; Chen, C.; Goldberg, I. H. *Biochemistry* **1988**, *27*, 4331–4340.

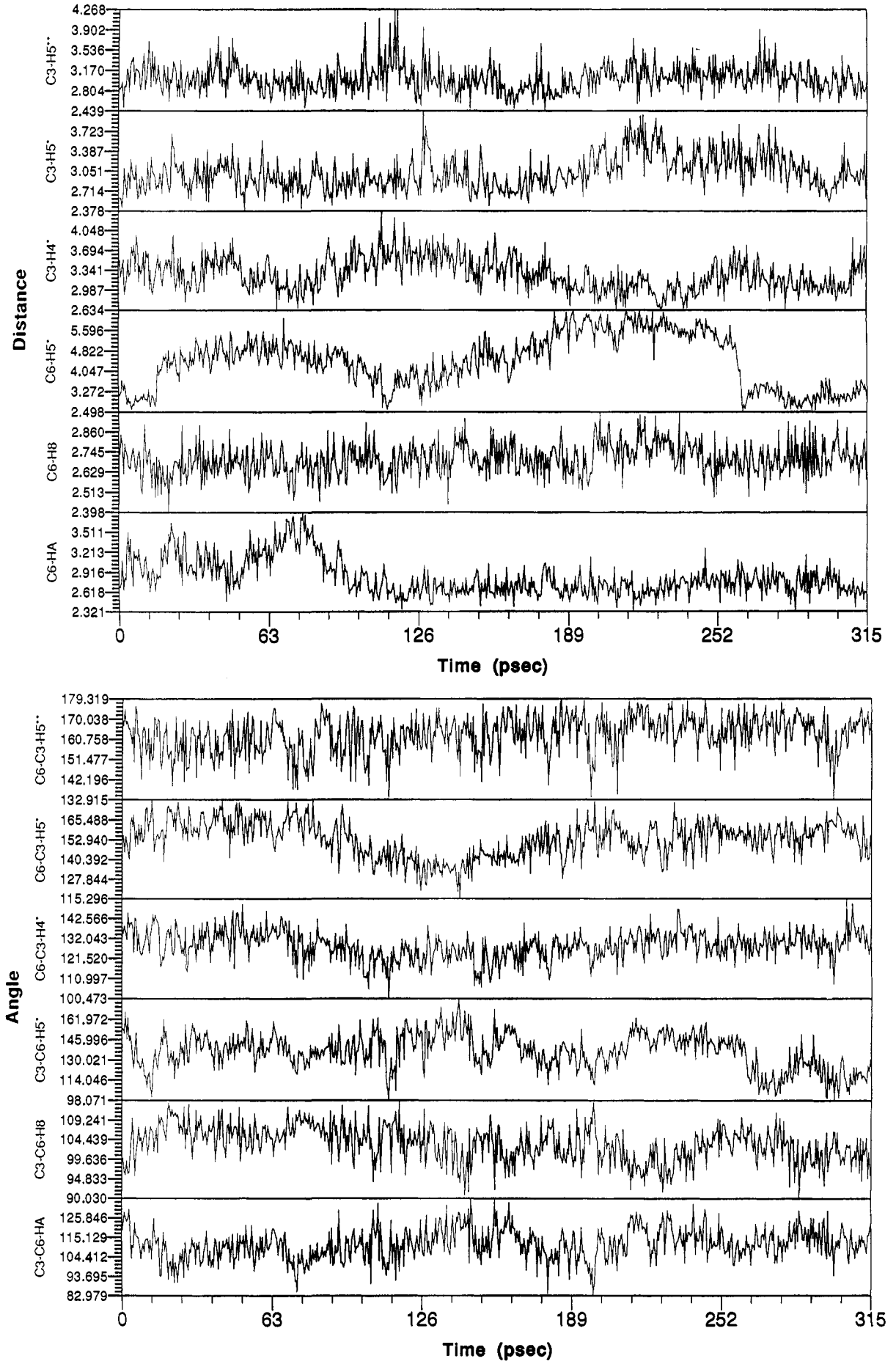

Figure 5. (top) Fluctuation in the distance (Å) between the esperamicin C3 and C6 radical centers and the three closest DNA or esperamicin hydrogens as a function of time. (bottom) Fluctuation of the C3–C6–Hx′ and C6–C3–Hx′ angles (degree) over time, where Hx = H5* of C:8 or H_8 or H_A of esperamicin and Hx′ = H5**, H5*, or H4* of T:17.

Scheme IV. Proposed Mechanism for the Homolytic Cleavage of the C8–O–Glycosidic Bond of Esperamicin Observed in the DNA–Cleavage Experiments

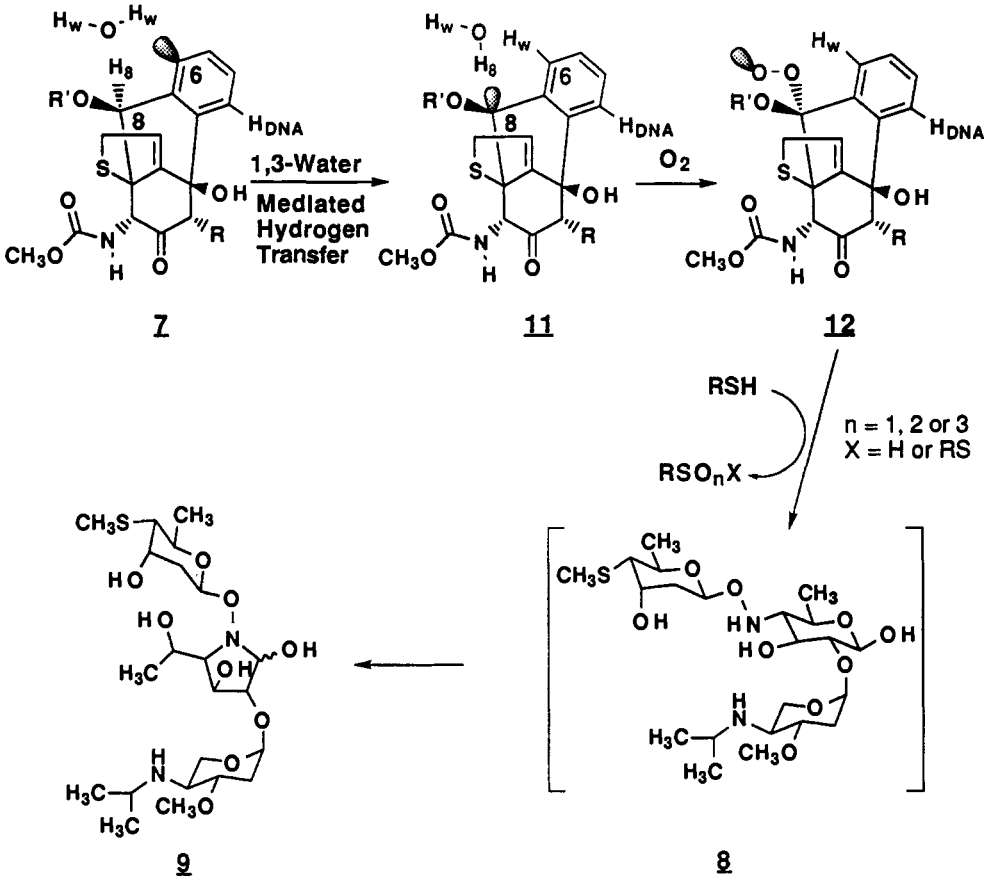

7 11 12 9 8

the carbinolamine (**9**), the major isolated esperamicin product from the DNA–esperamicin reaction.

The examination of the solvent in the region of the C6 radical revealed a highly ordered water molecule in the first hydration shell of the C:8 phosphate group. The ordered water molecule intermittently hydrogen bonds with the O2P of C:8 and O8, O2′, and O5‴ of esperamicin (Figure 6). This water is generally involved in two or more of these hydrogen bonds at a time, suggesting that it may play a structural role in the conformation of the DNA–drug complex. The water hydrogens are the closest and most directionally aligned to the C6 radical. Furthermore, the resultant hydroxyl radical would be well positioned to abstract the C8 hydrogen (Figure 7). The 1,3-water-mediated hydrogen transfer would produce the C8 radical (**10**, Scheme 3) and ultimately lead to the carbinolamine (**9**).

Summary of the Results

The biological activity exhibited by esperamicin is believed to arise from its ability to produce DNA strand breaks. Due to the short life span of the diradical,[96] esperamicin A_1 is presumably activated while bound to or at least very near the DNA. An examination of the DNA–esperamicin A_1 model (Figure 8) shows that the methyl trisulfide points into the surrounding environment, making it accessible for reductive activation. Once reduced the resulting thiolate can add in a Michael fashion to the β-position of the enone, removing the bridehead double bond. The removal of the anti-Bredt double bond in turn reduces the strain energy developed in the cycloaromatization reaction and allows for the formation of the diradical. The diradical can now abstract hydrogens from the host DNA and its environment.

The structure of esperamicin is uniquely designed to bind with DNA. It can readily adjust its conformation to adapt to its biological target. The deoxyfucose and anthranilate residues appear to be the least compromising. This is primarily due to the lipophilic character of the deoxyfucose and anthranilate, as well as the rigidity of the anthranilate. The rigidity and planar surface of the anthranilate are extended by the almost ever present hydrogen bond between the $C13^{iv}$ NH and $C7^{iv}$ carbonyl. The lipophilicity of deoxyfucose forces it to lie between the two phosphates at T:17 and G:18 and over the deoxyribose of T:17. This in turn fixes the position of the CORE and anthranilate in the minor and major grooves, respectively. The anthranilate makes and maintains VDW contacts with the major groove edge of bases T:17, G:18, and C:19 and the major groove face of the deoxyribose of T:17 and G:18. It is held in place by the deoxyfucose and stabilized by hydrogen bonds to O1P of T:17 and the 4-amino group of C:19. The position of the CORE in the minor groove is also stabilized by the intermittent hydrogen bonding of its C1-hydroxyl with O3* and O2P of T:16 and T:17, respectively, and with O12 of the CORE. However, the C1-hydroxyl spent most of its time interacting through a long-range hydrogen bond or water-mediated hydrogen bond with O5′ of the hydroxyamino sugar. The hydroxyamino sugar is indeed an unusual sugar in both its structure and its function. This sugar lies flat and floats two water layers above the floor of the minor groove. This mode of binding defies all conventional wisdom concerning DNA groove binders. The hydroxyamino sugar appears to function more as a scaffold from which the CORE and DNA-binding residues are attached than a DNA-binding element. The unusual binding orientation of the hydroxyamino sugar in the minor groove is governed by several factors. The most important guiding force is in the way the isopropylamino and thiomethyl sugars bind with the DNA. The isopropylamino sugar is a fairly hydrophobic sugar despite its amino group. Its lipophilic ring makes VDW contact with the deoxyribose of C:8, while the ammonium group forms a salt bridge with O1P of T:9. It is the binding position of the isopropylamino sugar that forces the hydroxyamino sugar to lie flat in the mouth of the minor groove.

(96) De Voss, J. J.; Hangeland, J. J.; Townsend, C. A. *J. Am. Chem. Soc.* **1990**, *112*, 4554–4556.

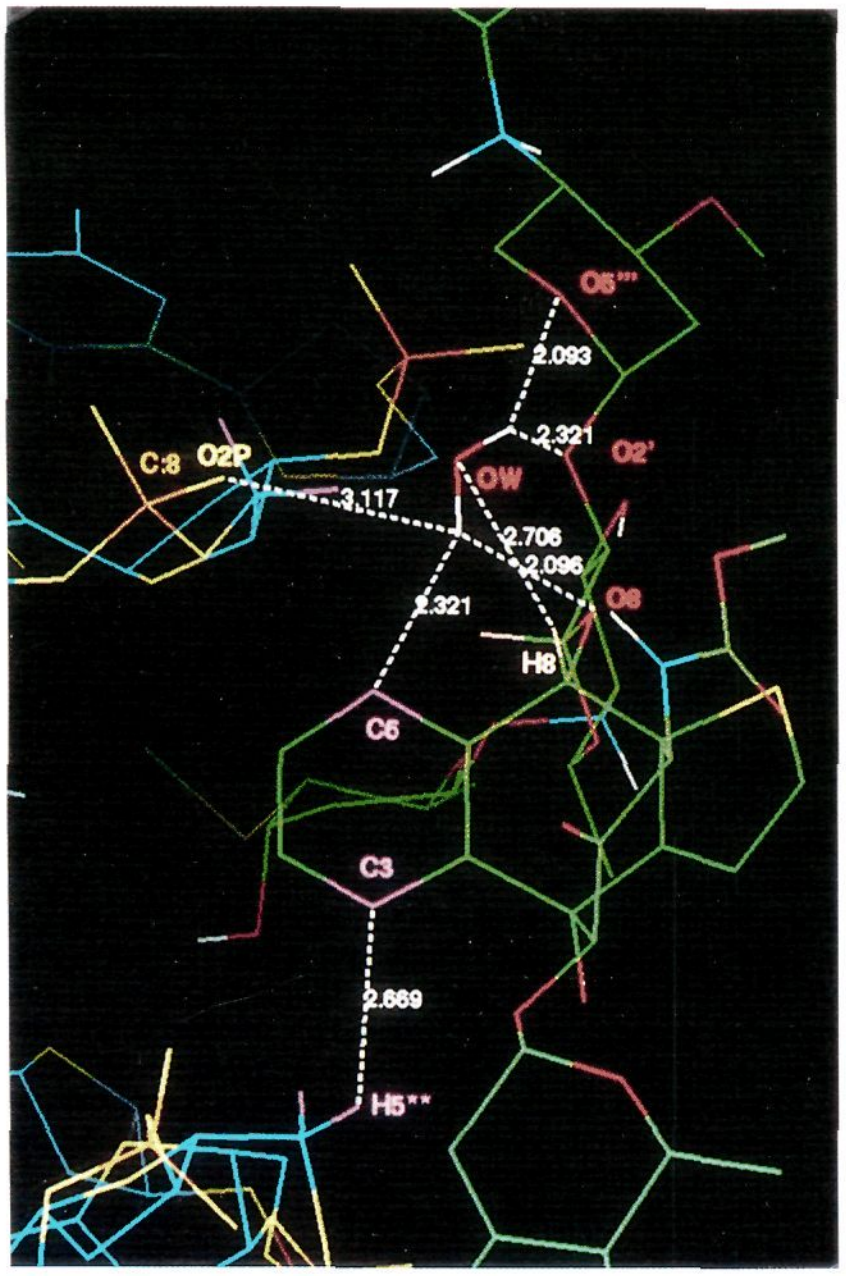

Figure 6. DNA–esperamicin ordered water molecule complex, a snapshot at 160ps.

The thiomethyl sugar is the most dynamic of all of the esperamicin residues. The planar surface of the thiomethyl sugar is sandwiched between the backbone atoms of the opposite strands of the DNA with its long axis pointing up and down the minor groove. It provides binding interaction, both VDW and hydrogen bonding, and it helps to orient the 1,4-axis of hydroxyamino sugar along the minor groove. The NO–glycosidic link between the hydroxyamino and thiomethyl sugars serves two important roles. It functions as an extended linker which allows the thiomethyl sugar to reach up the minor groove where it intermittently hydrogen bonds with O4* of A:15 or the 2-amino group and N3 of G:14. More importantly, the NO–glycosidic link allows the conformation of the hydroxyamino–thiomethyl disaccharide to adopt an energy minimum in which the two residues are orthogonal to one another. This minimum is stabilized by the 4'NH and C1'''O5''' antiparallel dipole.[66] The binding orientation of the hydroxyamino sugar in the minor groove is also stabilized by hydrogen bonds between the C3'-hydroxyl and O2P of T:9 and the hydroxyamino sugar O5' and CORE C1-hydroxyl. Another interesting interaction between the hydroxyamino sugar and the DNA comes from its 5'-methyl. This methyl provides VDW interactions with the deoxyribose of T:16 and may serve as the force that caused the minor groove to open slightly. The opening of the minor groove may be required to allow the esperamicin C and calicheamicin γ_1^I COREs to achieve binding positions in the minor groove that are suitable for simultaneous hydrogen abstraction from each strand of the DNA. The positions of the hydroxyamino sugar and deoxyfucose in the minor groove are critical, as they determine how the CORE sits in the groove.

The minor–major groove binding motif is supported experimentally by the affinity cleavage minor groove blocking studies[39] and osmium tetraoxide experiments.[68] In this mode, the drug binds to B-form double-stranded DNA and causes only minor perturbations in the DNA groove structure. While one face of the of the thymine C5–C6 double bond is sterically blocked by the DNA base to its 5'-side, due to DNA's right-handed helical twist, the 3'-face is approachable from the major groove in both naked and esperamicin C-complexed DNA. However, in the DNA–esperamicin A_1 complex, approaches to both the 5'- and 3'-faces of T:17 are completely blocked (Figure 4). It should also be noted that the minor groove and intercalative mode of binding offer no protection to the thymine double bond. In addition, the intercalative mode of binding disrupts the DNA groove structure in the vicinity of the intercalation site, causing both the major and minor grooves to widen. The intercalations of esperamicin A_1 into the 5'-ApA/3'-TpT step increase the exposure of the 3'-faces of T:16 and T:17 to the surrounding environment. Due to this disruption in the groove structure, one would not expect reduced levels of oxidation for the DNA–esperamicin A_1 complex but instead would predict higher or at best equal levels of oxidation when compared with naked DNA. However, it should be noted that the OsO_4 experiments have only given us information about the region of the DNA–esperamicin complex around thymine residues. Additionally, this study has focused on a single esperamicin binding site. For the above reasons, we cannot rule out the possibility of sequence-dependent modes of binding.

The CORE, deoxyfucose, and anthranilate act as a C-clamp around the deoxyribose of T:17, firmly planting the radical at C3 of the CORE for highly efficient hydrogen abstraction from C5* of T:17. However, the C6 radical is ill positioned for DNA hydrogen abstraction and is exposed to the solvent. The closest and most directionally aligned hydrogen is from a highly ordered water molecule. The quenching of the C6-radical to produce the hydroxyl radical is energetically disfavored by 4.22 kcal/mol (AM1-CI[97,98]); however, the caged hydroxyl radical is well positioned for abstraction of the C8-hydrogen of esperamicin. The overall reaction is favored by −28.94 kcal/mol and suggests a plausible mechanism by which the homolytic cleavage of the CORE C8-O–glycosidic linkage can occur. The resultant hemiacetal (**8**) after arrangement to an aldehyde and a Schiff base reaction with the NO–glycosidic linkage would produce the carbinolamine (**9**) form of the trisaccharide, the major isolated esperamicin product from the DNA–esperamicin cleavage reaction.

The esperamicin A_1 binding domain covers seven to eight base pairs in length (Table IA). To determine if there is a base preference at a particular location within the binding site, a population analysis was performed (Table IB,C). The strong esperamicin A_1 cut sites, as determined by the original researchers, were collected from the literature[39,50–57] and analyzed. The strong cut sites were categorized into 5'-(–B4–B3–B2–B1 Ct B1 B2) domains where B# is a purine (Pu) or pyrimidine (Py) base and Ct is the cut site. Only complete cut site domains were used in the analysis. The data (Table IB) shows 5'-N-Pu-Pu-Py-Py-N-Pu sequences, where N is either Pu or Py, to be hot spots for esperamicin A_1 cleavage. Out of the 67 strong cut sites, 16 (23.9%) agree with this finding while 32 (47.8%), 18 (26.9%), and 1 (1.5%) contain a single, double, or triple position mismatches, respectively. The 32 single mismatches are distributed into nonequal groups of –B1, B2 (7) > –B3, B2 (5) > –B2, B2 (3) > –B3, –B1 (2) > –B1, Ct (1). The single triple mismatch is at –B3, –B3, and B2. When the sequences are broken down into their respective bases, no one particular sequence stands out. Despite esperamicin's low sequence specificity, their appears to be an underlying preference for 5'-N-Pu-Pu-Py-Py*-N-Pu sequences, where N is either Pu or Py and Py* is the cut site. A single position mismatch at any location within the domain is well tolerated; however, esperamicin A_1 shows more sensitivity to double and triple site mismatches. The least tolerated multiple mismatches are the

(97) Steward, J. J. P. MOPAC, A Semi-Empirical Molecular Orbital Program, QCPE, 1983, p 455.
(98) Seiler, F. J. MOPAC 6.0, 1990.

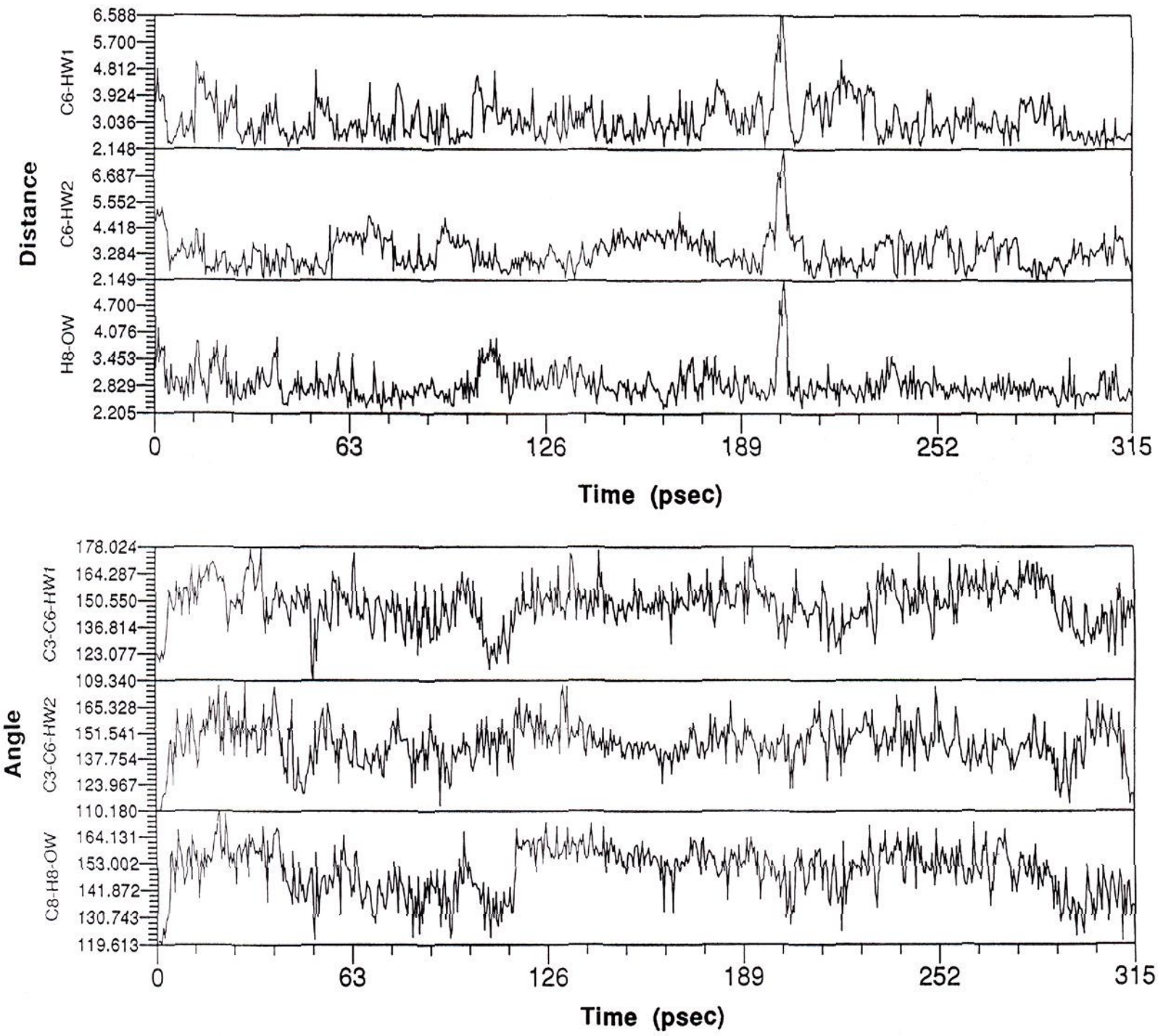

Figure 7. (top) Fluctuation of the C6-water hydrogens and H8-water oxygen distance (Å) over time. (bottom) Fluctuation of the C3-C6-water hydrogens and C8-H8-water oxygen angles (degrees) as a function of time.

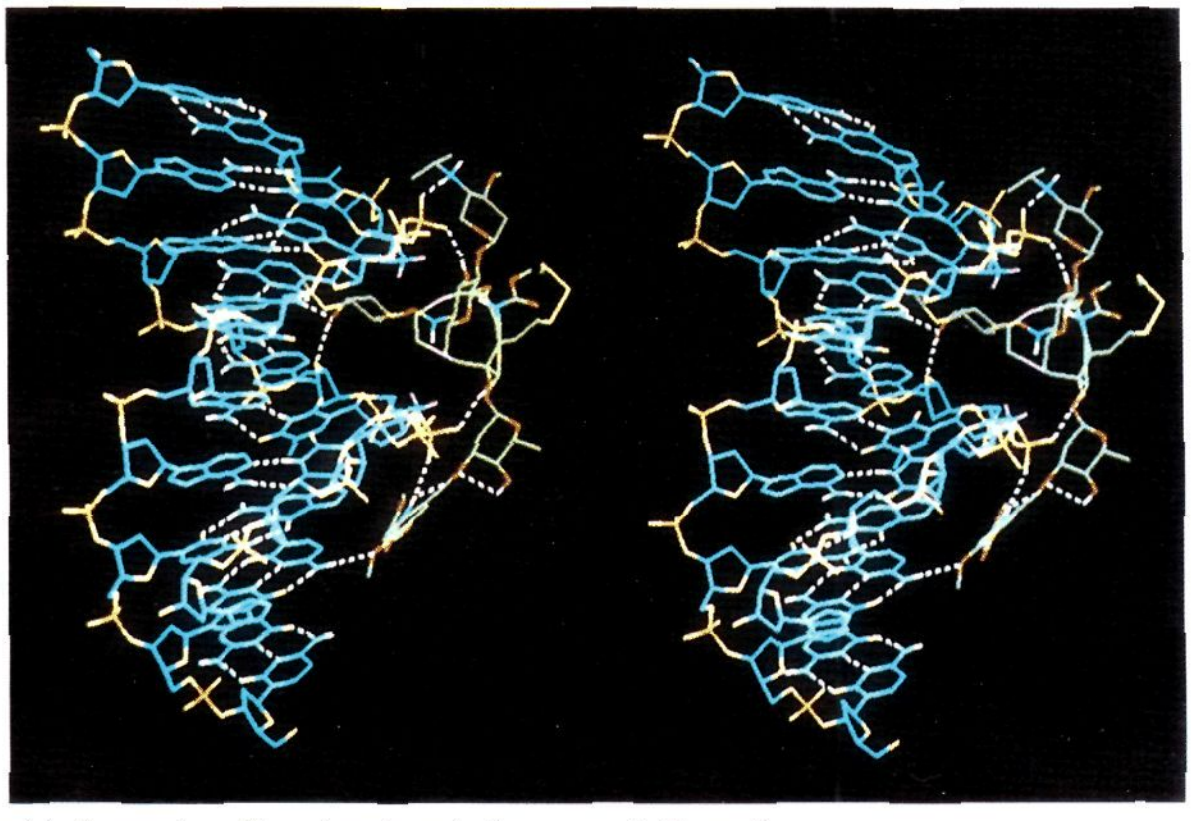

Figure 8. DNA–esperamicin A_1 complex. The color scheme is the same as in Figure 2.

ones in which the –B1 Ct sites are changed. The CORE and hydroxyamino sugar of esperamicin occupy the –B1 Ct region of the binding domain. They float one to two water layers above the floor of the minor groove and only directly interact with the DNA backbone. At first glance the reason for the –B1 Ct specificity is unclear, as the drug does not directly interact with the DNA bases. However, the spine of hydration that runs between the floor of the minor groove and the CORE and hydroxyamino sugar interacts with the drug and DNA in a specific manner that stabilizes the complex and positions the CORE for highly efficient DNA hydrogen abstraction. The nature of the spine of hydration that runs along the minor groove of DNA has been shown to be

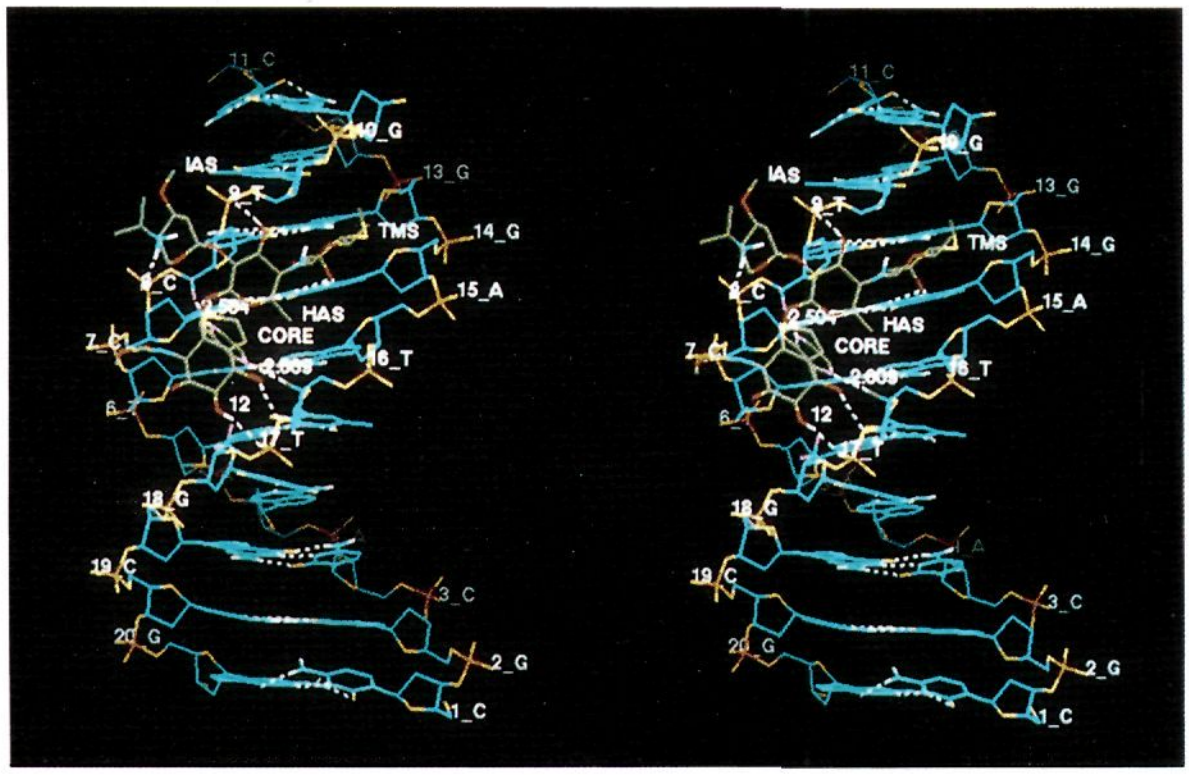

Figure 9. DNA–esperamicin C complex. The color scheme is the same as in Figure 2 with the addition of the green **H4*** T:16 hydrogen on the lower strand.

sequence dependent.[99,100] This study along with the DNA–esperamicin cleavage affinity experiments suggests that esperamicin maybe obtaining its sequence specific cleavage by reading the spine of hydration that runs along the minor groove. It is interesting to note that the cleavage specificity is not determined by the thiomethyl sugar and anthranilate. This is somewhat surprising, as one would expect the residues that make direct contact with the DNA bases to have the greatest influence in the determination of the binding specificity. This tends to make one suspect that high-affinity binding sites may not always be coincidental with cut sites. This suspicion is supported by the recent DNA-footprinting studies carried out on the aryl tetrasaccharide portion of calicheamicin.[45,46]

The pattern of DNA cleavage by esperamicin is directly related to its sequence specificity of cleavage. A given DNA cleavage site is often accompanied by a cleavage site on the opposite strand that is stagger by three bases in the 3′-direction. These staggered cut sites can be explained by considering the symmetry of –B3–B2–B1 Ct within the 5′-N-Pu-Pu-Py-Py*-N-Pu/3′-Pu-N-Py*-Py-Pu-Pu-N binding domain and a bidirectional mode of binding.[57] If the drug binds to the DNA with its trisaccharide tail pointing in the 5′-direction relative to the CORE and top strand of the DNA, then a cut site at the 3′-Py* in the top strand will ocurr. However, if the drug binds with the trisaccharide pointing in the 3′-direction relative to the top strand, the cut site will occur at the 3′-Py* of the bottom strand.

In order to further understand the single- versus double-stranded DNA cutting ability of esperamicin A_1 and esperamicin C, respectively, a model for the DNA–esperamicin C complex was constructed (Figure 9). Simply rotating about the C8–O–C1′ bonds positioned the CORE in the minor groove of the DNA so that the radicals at C3 and C6 are near and directionally aligned for the abstraction of the 4*-hydrogen from T:16 and 5*-hydrogen (*pro S*) from C:8, respectively (Figure 10). The concomitant abstraction of the H4* and H5* by C3 and C6, respectively, would produce a DNA double strand break with a three base pair stagger in the 3′-direction which is consistent with the observed cleavage pattern for esperamicin C[53–57] and calicheamicin.[40–44,48] The diradical-containing ring of esperamicin C points almost directly into the minor groove of the DNA (Figure 9), but more importantly, the C12-hydroxyl hydrogen bonds with O2P of T:17. For esperamicin A_1 to cause the same DNA strand breaks as esperamicin C, the deoxyfucose would have to occupy

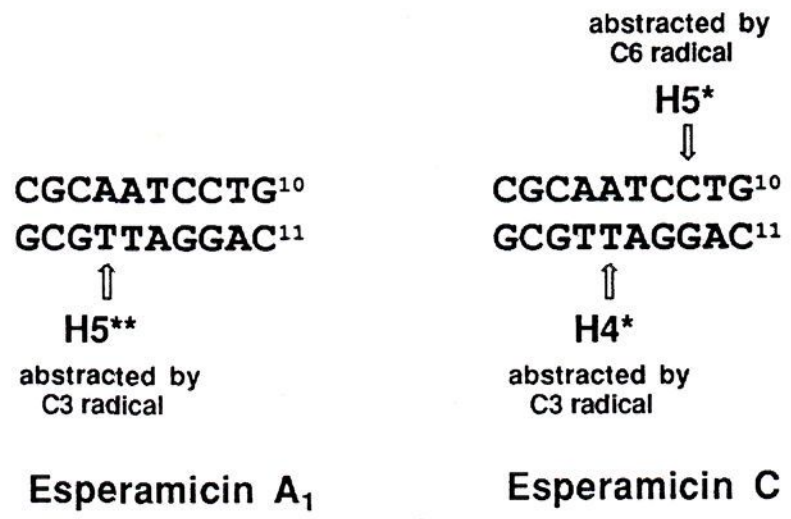

Figure 10. Predicted hydrogen atom abstraction pattern by esperamicin A_1 and esperamicin C when bound with their trisaccharide tails pointing in the 3′-direction relative to the top strand. It should be noted that the model slightly favors the abstraction of H5** over the H5* by esperamicin A_1; however, the abstraction of either of the C5* hydrogens is consistant with the available experimental data.

the same space as the T:17 phosphate group. Instead, the CORE of esperamicin A_1 is turned slightly in the minor groove, relative to esperamicin C, so that the deoxyfucose can sit between the phosphate groups of G:18 and T:17 and over the deoxyribose of T:17. The binding orientation of the esperamicin A_1 CORE within the minor groove positions the C3 radical for highly efficient hydrogen abstraction from C5* of T:17 (Figure 10), while the C6 radical is ill positioned for DNA hydrogen abstraction and ultimately leads to the fragmentation of esperamicin.

Conclusion

This simulation demonstrates the highly flexible and dynamical nature of DNA and how esperamicin's unique structure, stereochemistry, and substitution pattern give it the ability to slightly modify its conformation to accommodate its host.

The results provide an explanation of the function of the various components of the drug molecule and mechanism of action of esperamicin A_1 and esperamicin C which allows for a unified interpretation of the current experimental data.

The model places the enediyne moiety in the minor groove of the DNA in a way that positions the radical at C3 for highly efficient abstraction of a C5*-hydrogen from T:17. On the basis of this study, the H5** (*pro R*) is slightly favored over the H5* (*pro S*) as the most likely candidate for abstraction. Furthermore, it suggests a mechanism for the homolytic cleavage of the CORE

(99) Drew, H. R.; Dickerson, R. E. *J. Mol. Biol.* **1981**, *151*, 535–556.
(100) Kopka, M. L.; Fratini, A. V.; Drew, H. R.; Dickerson, R. E. *J. Mol. Biol.* **1983**, *163*, 129–146.

C8-O–glycosidic bond which involves a 1,3-water-mediated hydrogen transfer from C8 to C6.

The deoxyfucose forms a minor to major groove bridge over a deoxyribose and between two phosphate groups. This bridge causes the enediyne to turn slightly in the minor groove relative to the enediyne position found for esperamicin C and calicheamicin.[101] It is this slight difference in the enediyne binding position that leads to the different DNA-cleaving behavior expressed by these molecules.

The unusual hydroxyamino sugar lies flat in the mouth of the minor groove of the DNA and acts as a scaffold from which the other esperamicin residues are positioned for optical interaction with the DNA host. The NO–glycosidic linkage functions as a linker between hydroxyamino and thiomethyl sugars and allows them to adopt an orthogonal geometry relative to one another and extends the reach of the thiomethyl sugars along the minor groove.

The model also predicts that esperamicin binds predominantly with the DNA backbone, which explains its low absolute sequence specificity. This suggests that it should be possible to use carbohydrates as well as other organic moieties that interact via van der Waals and electrostatic interactions with the DNA backbone to increase the binding constant (potency) of other potentially useful drugs (including antisense and triple-helix DNA) without affecting their sequence specificity.

The minor–major groove binding motif of esperamicin A_1 is more reminiscent of the binding modes of the CRO and λ repressors[102] than that observed for other non-protein DNA-binding molecules. It is the first nonintercalating natural product that binds simultaneously in both the minor and major grooves of the DNA and provides the first clue from nature in how to design a hybid minor–major groove binders.

Experimental Section

Reaction of Esperamicin A_1 with CT-DNA. To a vigorously stirred sample of CT-DNA (18.5 mg) in 10 mL of 0.05 M Tris·HCl buffer (pH = 7.8) and 1 mL of absolute ethanol was added esperamicin A_1 (4.8 mg in 0.5 mL of ethanol) followed by 45 μL of methylthioglycolate. The reaction mixture was stirred at 37 °C for 3 h with occasional sonication. After that time, the ethanol was removed by evaporation at 37 °C under vacuum. The resultant aqueous solution was then freeze dried. The residue was extracted with methylene chloride (2 × 25 mL). The solvent was evaporated to dryness, and the residue was redissolved in 3 mL of dry methanol. The methanol solution was acidified with 100 μL of glacial acidic acid and stirred at room temperature for 24 h. The major product (1.1 mg, yield ca. 60%) was isolated by TLC (20- × 20- × 0.025-cm silica gel plate in $CHCl_3$:MeOH (5:0.8, v/v)) and identified by MS and NMR as the α-methyl glycoside of **9** (Scheme 2) previously obtained by reduction of esperamicin A_1 with $NaBH_4$.[33]

Footprinting of Bound Esperamicins A_1 and C.[68] The synthesis, purification, and annealing of the oligonucleotide (Figure 3) have been reported elsewhere.[55] The oligonucleotide in the absence or presence of 2-fold esperamicin A_1 or C was incubated with 1 mM osmium tetraoxide and 3% pyridine in 50 mM Tris·HCl, pH 7.5, and 10 mM $MgCl_2$ in a 20-μL final volume at 18 °C for 10 min.[69] The reactions were stopped by two sequential ethanol precipitations and then lyophilized. The DNAs were cleaved at the sites of osmate adducts by treatment with 100 μL of 1 M piperidine at 90 °C for 30 min, followed by extensive lyophilization. Sequencing and gel electrophoresis were carried out as described elsewhere.[55]

Acknowledgment. We would like to thank Dr. G. Ravishanker for many useful discussions on molecular dynamics and analysis of the results. We also thank Drs. M. Lu, Q. Guo, and N. R. Kallenbach for sharing their unpublished results. This work was supported by grants to D.L.B. from the National Institutes of Health (GM-37909) and from the Bristol-Myers Squibb Company via a Connecticut Cooperative High Technology Research and Development Grant.

Supplementary Material Available: Complete Curves, Dial, and Windows[86] graphical analyses on all the DNA parameters over the time course of the molecular dynamics simulation (24 pages). This material is contained in many libraries on microfiche, immediately follows this article in the microfilm version of the journal, and can be ordered from the ACS; see any current masthead page for ordering information.

(101) Langley, D. R.; Doyle, T. W.; Beveridge, D. L. *Tetrahedron Symposia in Print*, **1993**, in press.

(102) Anderson, W. F.; Ohlendorf, D. H.; Takeda, Y.; Matthews, B. W. *Nature* **1981**, *290*, 754–758.